

THESIS FOR THE DEGREE OF DOCTOR OF
PHILOSOPHY

Multi Quanta Relaxation
and Nonclassicality of Nonlinear
Oscillators

AURORA VOJE



CHALMERS

Department of Applied Physics
CHALMERS UNIVERSITY OF TECHNOLOGY
SE-412 96 Göteborg, Sweden 2014

Multi Quanta Relaxation and Nonclassicality of Nonlinear Oscillators

AURORA VOJE

ISBN 978-91-7597-110-0

©Aurora Voje, 2014

Doktorsavhandling vid Chalmers Tekniska högskola

Ny serie nr 3791

ISSN 0346-718X

Condensed Matter Theory
Department of Applied Physics
Chalmers University of Technology
SE-412 96 Göteborg
Sweden
Telephone +46 (0)31 772 1000

Printed by Chalmers Reproservice
Chalmers University of Technology
Göteborg, Sweden 2014

Typeset in L^AT_EX. Figures created using MATLAB, Inkscape and POV-Ray.

Cover: Wigner function in phase space of position and momentum of a finite temperature steady state created by nonlinear damping.

Multi Quanta Relaxation and Nonclassicality of Nonlinear Oscillators

AURORA VOJE

Condensed Matter Theory

Department of Applied Physics

Chalmers University of Technology

ABSTRACT

The focus of the study is the free quantum evolution of Duffing oscillators which are nonlinearly coupled to bosonic environments. The work evolves from a particular system of an undamped, nonlinear graphene resonator mode to a more generalized framework of oscillator modes interacting with two different configurations of bosonic environments. In a model with no dissipation, the nonlinear Duffing oscillator allows an initial coherent state to evolve into a macroscopic superposition state, a Schrödinger Cat state. By further subjecting a Duffing mode to nonlinear damping, the parity conservation due to the two-quanta system-bath exchange, brings the system to a nonclassical steady state - an equilibrium state very much different from the ground state. The quantum features of this state are analysed for temperatures above zero and in a more realistic scenario where the interplay of linear and nonlinear decay is taken into account. The scope of the study is then extended to bipartite systems of nonlinear interacting oscillators, each nonlinearly coupled to a bosonic environment. The generation of entanglement in initially separable states and entanglement's asymptotic behaviour are investigated. One of the outcomes is the Duffing nonlinearity not affecting the entanglement asymptote. Therefore, finally a bipartite system of harmonic oscillators, with nonlinear system-bath coupling is initiated with entangled, squeezed states, and the asymptotic behaviour is evaluated in the parameter space of temperature, squeezing and dissipation rate. This is done for common and individual reservoir configurations, and either zero or non-zero inter-mode coupling.

Keywords: Quantum Duffing Oscillator, Nonclassical States, Nonlinear Damping, Entanglement

This thesis is based on the research outcomes of paper I-IV.

PAPER I

Generating Macroscopic Superposition States in Nanomechanical Graphene Resonators

A. Voje, J. M. Kinaret and A. Isacsson.
Physical Review B **85**, 205415 (2012)

PAPER II

Multi-Phonon Relaxation and Generation of Quantum States in a Nonlinear Mechanical Oscillator

A. Voje, A. Croy and A. Isacsson.
New Journal of Physics **15**, 053041 (2013)

PAPER III

Nonlinear-dissipation-induced Entanglement of Coupled Nonlinear Oscillators

A. Voje, A. Isacsson and A. Croy.
Physical Review A **88**, 022309 (2013)

PAPER IV

Entanglement Dynamics of Quantum Oscillators Nonlinearly Coupled to Thermal Environments

A. Voje, A. Croy and A. Isacsson.
arXiv:1412.1999 (2014)

Contribution Report

The author has on all papers contributed with numerical and theoretical analysis, as well as with manuscript preparation.

Other scientific contributions

Mechanical Cat States in Graphene Resonators

A. Voje

Licentiate Thesis, Chalmers University of Technology (2012)

Nonlinear Conductivity in Coulomb Glasses

M. Caravaca, A. Voje, J. Bergli, M. Ortuno, and A. M. Somoza

Ann. Phys. **18**, 12 (2009)

TABLE OF CONTENTS

Research Publications	i
1 Embracing the Quantum Nature	3
1.1 Probing the Quantum with Light	3
1.2 Quantum NEMS	5
2 The Quantum Mechanical Realm	11
2.1 Modelling the Nature By Oscillators	12
2.1.1 The Beloved Harmonic Oscillator	12
2.1.2 The Duffing Oscillator	16
2.2 State Superposition and Entanglement	18
2.2.1 Entangled States	20
2.2.2 Classification and Quantification of Entanglement	22
3 Dissipation	25
3.1 Classical Dissipation	25
3.2 Quantum Dissipation	27
3.2.1 Linear Coupling	28
3.2.2 Nonlinear Coupling	32
4 Summary of Appended Papers	35
4.1 Paper I	35
4.2 Paper II	41
4.3 Paper III	45
4.4 Paper IV	47
5 Conclusion	49
6 Acknowledgements	51
A The Wigner Function	53
A.1 The Moyal Function	54
A.2 Wigner Function for two Harmonic Oscillators	56
B Rotating Wave Approximation	58

C	Evolution of a Coherent State in a Duffing Potential	60
D	Quantum Master Equations	62
D.1	Linear Coupling	64
D.2	Nonlinear coupling	66

Dear reader, it is an honour that you are looking through this thesis, especially if it is by your own will. The main purpose of this work is to share the knowledge acquired during the PhD studies in an understandable manner with a mixed audience in mind. This is a challenging task. My intention was therefore to construct this thesis according to the funnel structure. A typical funnel is initially wide and gradually focuses towards a narrow end.

Correspondingly, this thesis begins with chapter 1 which is devoted to the broader introduction of the scientific background, motivating the questions and problems of my own research. This chapter summarises the development of the experimental work probing quantum mechanics in several branches of physics, focusing towards the nanoelectomechanical systems. The dynamics of such systems are modelled by oscillators. The following chapter 2 and chapter 3 consider some relevant theoretical concepts of quantum oscillator dynamics in closed systems and in systems interacting with an environment. The contents of these chapters should be comprehensible to physics students.

Finally, the focus narrows down to the study comprised in the appended research papers. A brief summary of the most important outcomes is given in chapter 4, and the publications can be found appended at the end of the thesis. The most relevant calculations of the previous chapters are included as appendices, which follow after the concluding remarks in chapter 5 and acknowledgements.

Below you will find a list of abbreviations used throughout the thesis. The list is in alphabetical order.

List of Abbreviations	
CV	Continuous Variable
EPR	Einsten Podolsky Rosen
ESDR	Entanglement Sudden Disappearance and Revival
LD	Linear Damping
LHVM	Local Hidden Variable Model
NEMS	Nanoelectromechanical Systems
NLD	Nonlinear Damping
PPT	Positive Partial Transpose
QME	Quantum Master Equation
QNEMS	Quantum Nanoelectomechanical Systems
RWA	Rotating Wave Approximation

CHAPTER 1

Embracing the Quantum Nature

Our understanding of nature is dynamic and changes as new discoveries are made and ideas evolve. In physics, a paradigm shift in the description of the microscopic world took place in the early 20th century. Reports of *e.g.* atomic emission spectra, black-body radiation [1] and the photoelectric effect [2, 3], unexplainable in terms of existing, deterministic Newtonian mechanics and classical electrodynamics, pushed the greatest minds of that time to a new level of comprehension.

Ever since its emergence, the quantum theory has been probed experimentally in various fields of physics. In this chapter a short tour through some of the most important results of quantum state engineering in the area of quantum optics and quantum nanoelectromechanical systems (NEMS) will be given. It is natural to begin with shining light on the area of quantum optics, which during the last seventy years has had a fantastic development with respect to experimental verification of quantum mechanics [4]. Quantum optics also provides a wide range of theoretical achievements [5], which can be further implemented in the quantum description of systems in other areas of physics.

1.1 Probing the Quantum with Light

"Quantum optics covers quantum phenomena in the radiation-atom interaction [...], it is also an arena in which to illustrate and elucidate quantum effects." [7] The successful development of quantum optics grew in parallel with advancement of *e.g.* laser spectroscopy, quantum state detection methods [8], and faster computers monitoring data sampling, to mention a few [7]. Specifically, the excited Rydberg atoms [9] and the invention of the micromaser [10], were important ingredients in quantum optical state engineering. Implementation of these results led to beautiful experiments by the groups led by S. Haroche and D. Wineland, enabling tests of the "Gedanken experiments" of quantum superposition and entanglement, which one only could dream about in the early 1900. These achievements were awarded by the Nobel Prize in 2012, acknowledging the scientific importance of the field [6, 11]. By trapping individual ions and isolating single quantized field modes (photons), controlled creation and manipulation of superpositions of photonic and phononic quantum states, such as Schrödinger

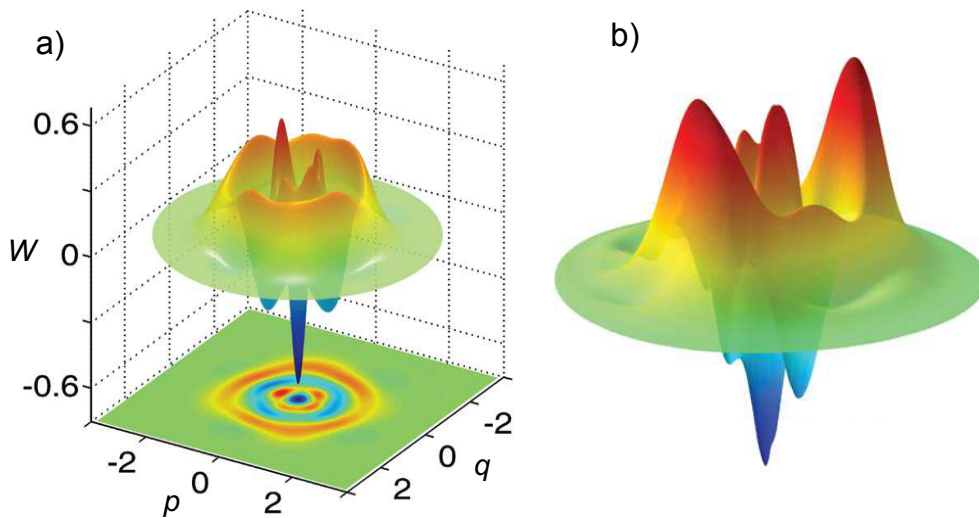


Figure 1.1: a) The experimental Wigner distribution W of a number state $n = 3$ in phase space of position q and momentum p . b) The experimental Wigner distribution of a Schrödinger Cat state. The figures are from [6].

©The Nobel Foundation 2012, S. Haroche.

cat states¹, became possible [12, 13].

Figure 1.1 is taken from the awarded work of S. Haroche [6] and shows the experimentally derived Wigner distribution of quantum states of radiation. Figure 1.1 a) and b) are non-classical states which will be more discussed in chapter 2. The Wigner distributions were experimentally obtained by tomographic field state reconstruction, often called Wigner tomography [14]. This is a reconstruction technique, based on statistical, non-destructive, measurements of the state, where coherences of the state's number distribution are obtained. The visualization of the state is given in terms of the Wigner distribution function. In his Nobel lecture S. Haroche gives a good analogy to what a Wigner function represents: "The Wigner function is to the density matrix what the hologram is to the direct image of an object." [6].² A detailed description of the Wigner function can be found in chapter 2 and Appendix A. Engineering of quantum states goes hand in hand with their verification, and Wigner tomography is an important ingredient in this process.

In Haroche's experiments the entanglement between matter and radiation is an important element. Entanglement considers non-classical correlations between spatially separated systems. The importance of its exploration is manifested in

¹The mentioned quantum states will be discussed in more detail in the following chapters.

²The density matrix holds the information of the quantum state. A direct image is equivalent to a photograph.

the emergence of a new branch in physics - the quantum information theory. The experimental investigation of the entanglement phenomenon originally belonged to the quantum optical domain [15], but has over the years progressed to other structures like *e.g* spin and solid state systems [16]. Recently entanglement of a mechanical resonator and an electrical signal was demonstrated [17], by this extending the domain of accessible quantum information resources to macroscopic, nanoelectromechanical systems (NEMS).

1.2 Quantum NEMS

As the experimental techniques progressed, so did the drive towards creation of quantum states in bigger objects. Various research groups have succeeded with superposing states of Cooper pairs in superconductors [18], molecules like the C_{60} fullerene [19], depicted in figure 1.3 c), and large organic molecules [20], even viruses are proposed for a trial [21] Larger objects in which superposition states can be created are represented by the nanoelectromechanical systems (NEMS). These are nano- and micrometer-sized resonator devices like doubly clamped beams, cantilevers, membranes, toroids and mirrors. In these devices one wishes to detect the quantum motion and make the resonators simultaneously vibrate in two states. An observation of this kind in human designed objects is considered a scientific milestone.

The Race Towards Quantum Motion.

In order to generate macroscopic quantum states in mechanical resonators, one must be able to control them at the level of individual quanta. During the first decade of the 21st century there was a "hot pursuit" race between several experimental groups with the goal of demonstrating controlled quantum motion and reaching the ground state in NEMS. In 2003 Science magazine estimated that within a half year time the quantum limit would be reached and obtaining superposition states in NEMS would be possible. The estimate turned out to be too ambitious.

To enter the quantum regime the temperature dependent thermal energy, $k_B T$, is required to be smaller than the quantum energy level spacing, $\Delta E_n = \hbar\omega$, of a resonator with frequency ω . The resonator is to the lowest approximation assumed to behave as a harmonic oscillator, which is the backbone model for the resonators. For a harmonic oscillator the energy spectrum is given by $E_n = \hbar\omega(n + 1/2)$, where n is the occupation number. An occupation number of $n = k_B T / \hbar\omega - 1/2 < 1$, indicates that the resonator is in its ground state. To reach the ground state the system must be cooled down to temperatures close to absolute zero. Even at absolute zero temperature no object stands perfectly still, but is subject to quantum fluctuations in position q and momentum p , satisfying

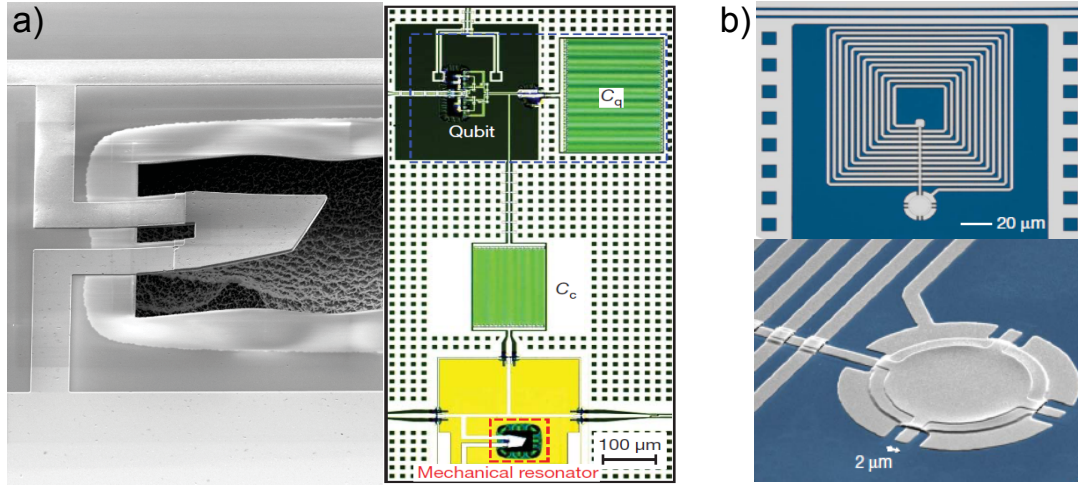


Figure 1.2: The first two NEMS resonators where the quantum ground state is reached and verified. a) Left: The mechanical oscillator with oscillations of its volume. Right: The full system set-up where the mechanical oscillator is coupled to a qubit, which enables the readout of the oscillator's state. Reprinted by permission from A. N. Cleland, Nature [22], copyright (2010). b) Zoom of the mechanical oscillator membrane, part of an LC-circuit, strongly coupled to a microwave cavity. Reprinted by permission from J. D. Teufel, Nature [23], copyright (2011).

the Heisenberg uncertainty principle $\sqrt{\langle \Delta \hat{q}^2 \rangle \langle \Delta \hat{p}^2 \rangle} \geq \hbar/2$. The uncertainty principle, which will be discussed in chapter 2, relates to the resonator's zero point motion. Detection of the zero point motion is a desirable proof of reaching the ground state, but measuring it is in practice far from trivial. The challenges lie within system cooling and state readout. While it is possible to cool a NEM resonator to the ground state using only a cryostat [22], most schemes additionally involve active cooling techniques [24, 25]. Measurement of a quantum system will always disturb it in some sense. This is called backaction. To achieve a successful, continuous quantum state readout, backaction evading measurement techniques must be implemented into the experimental set-up [8, 25].

Overcoming the challenges in reaching the quantum ground state and successfully measuring it, was first accomplished in the year 2010 by Andrew Cleland's group [22]. This breakthrough was achieved by coupling a mechanical resonator, with oscillations of its volume, to a two-level qubit system. The response of the qubit is affected by the occupation of the mechanical resonator. The state of the resonator can therefore be probed by measuring the response of the qubit. The picture of the mechanical resonator and the experimental set-up is shown in figure 1.2 a). In 2011 Teufel *et al.* managed to cool a mechanical resonator drum to such low temperatures that it seldom left its ground state [26]. The

drum was a part of a superconducting circuit which was strongly coupled to an optical cavity. Via side-band cooling, emission of the resonator energy into the cavity enabled an efficient reduction in resonator's temperature. The picture of the resonator drum is shown in figure 1.1 b). As mentioned in section 1.1 this system was later implemented to create entangled two-mode squeezed states of the mechanical and microwave oscillators.

Carbon based NEMS and The Era of Graphene

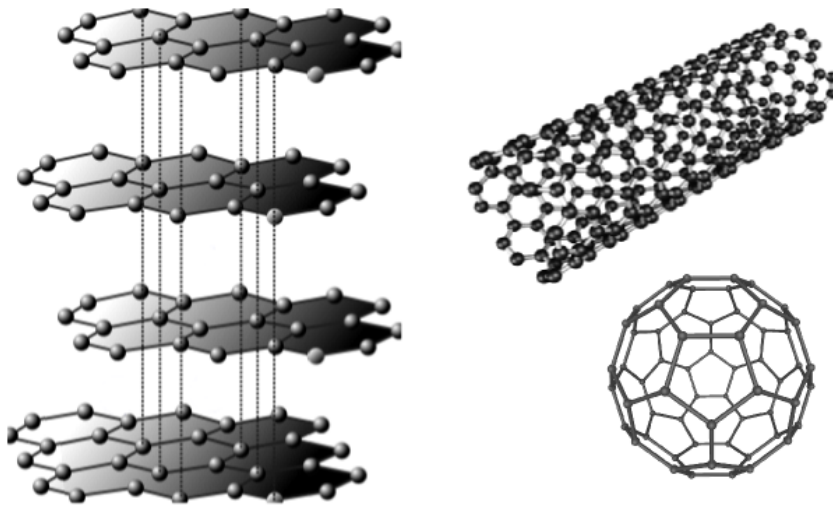


Figure 1.3: Schematic representation of three carbon allotropes. a) Four layers of graphene. When stacked upon each other, multiple layers of graphene constitute graphite. b) Graphene can also be cut and rolled into a carbon nanotube. c) The C_{60} fullerene is another carbon allotrope.

Figure source: wikipedia/commons

The nano-resonators mentioned in the previous section typically vibrate at frequencies of the order of a gigahertz, which results in energy quanta of the order of millikelvin. To vibrate that fast, the size of the resonator has to be reduced. A drawback of the small micro-fabricated resonator beams and drums is the decrease of their quality factor together with their size. The Q -factor is a measure of how much of the energy stored in the resonator is lost to the environment per cycle $Q \sim E_{\text{in}}/E_{\text{out}}$. A low Q -factor means the resonator rapidly dissipates energy, which is unfortunate with respect to the coherence of a quantum state. The lower the Q -factor, the faster the system decoheres, and the more difficult it is to perform measurements on it. It has been observed that carbon-based nanoresonators like carbon nanotubes and graphene membranes provide high Q -factors [27, 28]. This combined with a small mass and high strength makes them good NEMS resonator candidates with a detectable zero point motion, if put

into quantum regime.

The carbon nanotube shown in figure 1.3 b), emerged as a hot topic in solid state physics in the 90s, with scientific visions and dreams regarding many an application. In 2003-2004 isolation of a single-layer graphene by "the scotch tape technique" was reported [29]. Since then graphene and the nanotube have shared the role of the hot material science topic [30]. The existing, relatively broad knowledge about the nanotubes accelerated the progressing graphene research. At the moment graphene is attractive both for academic and industrial purposes. In 2010 the Nobel Physics prize was awarded to A. Geim and K. Novoselov for their ground breaking experiments with graphene.³ In one of his Nobel lectures at Chalmers University of Technology, A. Geim claimed; "For a material an average journey from academia to industry takes several decades. For graphene it only took several years."

Graphene is a mono layer of carbon atoms arranged in a two-dimensional hexagonal (honeycomb) lattice and is a very light material. When many layers of graphene are stacked on top of each other they are held together by the weak van der Waals forces, and constitute graphite. Four layers of graphene are shown in figure 1.3 a). Most of us have encountered graphite through writing or drawing with a pencil. Due to the covalent atomic bonds graphene is strong, yet flexible. It is elastically stretchable up to 20%, which is very large compared to other crystalline materials. Additionally, it is transparent and has ballistic electron transport, making it interesting for optical and electronic implementations [31]. The deflection in response to an applied force is nonlinear when graphene's out of plane deflection exceeds its thickness. The nonlinear response occurs at small deflection amplitudes [32], and tension induced nonlinear effects allow to tune its resonance frequency [33, 34]. These nonlinear effects are attractive features with respect to the quantum regime, as a nonlinear quantum oscillator exhibits features which do not exist in the classical dynamics [35].

For graphene one of the experimental challenges in reaching the quantum regime is to create sufficiently large coupling to a readout mechanism. By now several successful optomechanical setups, where the graphene flake plays the role of a capacitor plate in the integrated circuit, its flexural motion changing the capacitance, enabling optical cavity readout, are promising with respect to reaching the quantum regime [36, 37, 38]. At the moment, the lowest number of mechanical quanta in graphene's fundamental mode is about 50 [37].

Another interesting factor in recent experimental reports is graphene and carbon nanotubes displaying nonlinear dissipation (NLD), when they are under tensile strain [28]. The damping depends strongly on the amplitude of resonator's

³For about 60 years graphene was theoretically studied, and considered a theoretical material, as it was presumed not to exist in a free state.

motion, and the authors attribute NLD to clamping losses or linear damping mechanisms coupled to geometric nonlinearities. It has also been proposed that NLD in graphene occurs due to coupling between flexural and in-plane motion [39]. There are several numbers of studies of NLD in NEMS [40], quantum optical [41, 42], optomechanical [43] and solid state [44] systems underlining the importance and relevance of its theoretical and experimental exploration. In chapters 3 and 4 further discussion on NLD, and how it affects a nonlinear resonator in quantum regime will be picked up.

CHAPTER 2

The Quantum Mechanical Realm

In this chapter the basic concepts of quantum mechanics will be briefly explained and angled towards the upcoming chapters. Theory-wise this chapter will correspond to "dipping the toes into the vast ocean".

Consider an object which is confined to a potential in one dimension, like the harmonic oscillator. When a localized system is investigated in the quantum regime its observables such as energy, position and momentum are quantized. In contrast to classical scalar system observables, the quantum observables are described by matrices with probability weighted measurement outcomes, called eigenvalues. The entire information of the system is encoded in the wave function $|\psi\rangle$, expanded in a basis which spans the Hilbert space¹. The evolution of $|\psi\rangle$ of a closed quantum system, *i.e.* when there is no environment interaction, is described by the Schrödinger equation

$$i\hbar\partial_t|\psi\rangle = \hat{H}|\psi\rangle, \quad (2.1)$$

where \hat{H} is the Hamiltonian, the system's energy operator.

If $|\psi\rangle$ is constructed such that when acted on by an operator \hat{O} it remains unchanged, then $|\psi\rangle$ is called an eigenfunction of the operator \hat{O} . If two operators do not have a common set of eigenfunctions, they can not be simultaneously observed with an unlimited precision. The limit is set by the Heisenberg uncertainty principle. A standard example of this principle can be illustrated by the position and momentum operators \hat{q} and \hat{p} . The uncertainty principle states that the product of their quantum fluctuations is

$$\sqrt{\langle\Delta\hat{q}^2\rangle\langle\Delta\hat{p}^2\rangle} \geq \hbar/2. \quad (2.2)$$

Hence a precise observation of one observable quantity means decreased precision in the observation of the other. The uncertainty principle is an important ingredient in both the theoretical and experimental investigation of quantum systems.

¹The Hilbert space is a complete inner product space.

2.1 Modelling the Nature By Oscillators

Physicists love to describe systems in terms of harmonic oscillators, as the harmonic model is a solvable and expandable generic model. In the upcoming section the free evolution of an ideal system of a harmonic oscillator will be described. The classical picture is first presented and subsequently compared with the quantum mechanical representation. A similar approach is then repeated for a special anharmonic oscillator, the Duffing oscillator.

2.1.1 The Beloved Harmonic Oscillator

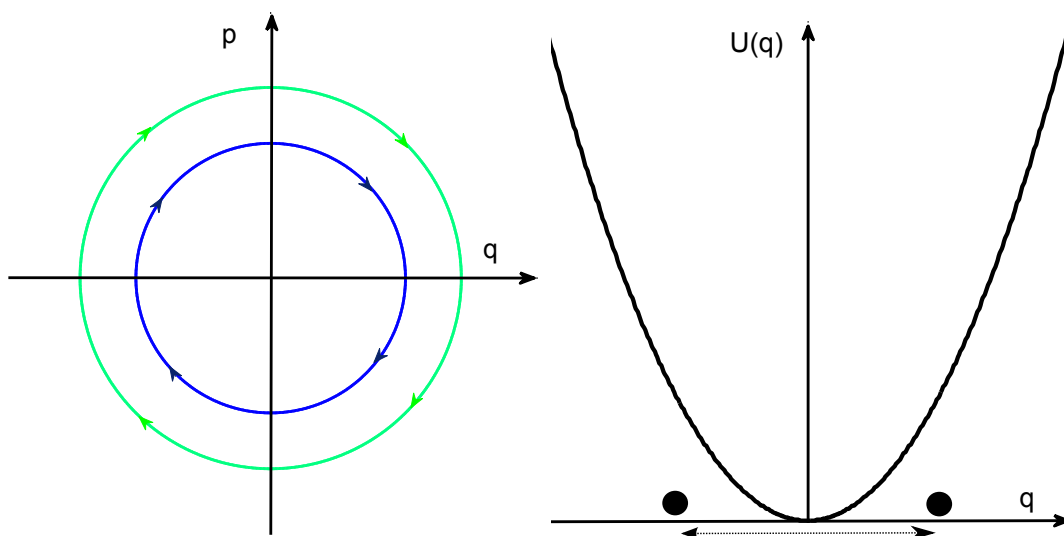


Figure 2.1: a) Classical, free evolution of the harmonic oscillator in the phase space of position and momentum (q, p) . Circular trajectories visualize constant oscillator energies. b) Schematic representation of a classical harmonic oscillator swinging back and forth in a harmonic potential $U(q) = m\omega^2 q^2/2$. The classical harmonic oscillator has a continuous energy spectrum, and amplitude independent frequency.

The classical expression for the total energy E of a harmonic oscillator is given in terms of the sum of the kinetic and potential energy

$$E = \frac{p^2}{2m} + \frac{1}{2}m\omega^2 q^2. \quad (2.3)$$

Here q is the oscillator position and p is its momentum. All the measurable variables are scalars, which vary continuously. The oscillator frequency is given by $\omega = \sqrt{k/m}$, where k is the spring constant, and m is the oscillator's mass. Imagine now displacing the oscillator from its equilibrium, and letting it swing back and forth about its equilibrium. The free evolution of such ideal oscillator

in the phase space of (q, p) is shown in figure 2.1 a). The amplitudes of (q, p) are frequency independent and the total energy is conserved, as indicated by the circular trajectories. Figure 2.1 b) is a schematic representation of the oscillator swinging back and forth about its equilibrium in the harmonic potential.

In the quantum mechanical representation of a harmonic oscillator the total energy is given by the Hamilton operator \hat{H} which is a sum of the kinetic and potential energy, respectively expressed in terms of position and momentum operators \hat{q}, \hat{p}

$$\hat{H}_0 = \frac{\hat{p}^2}{2m} + \frac{1}{2}m\omega^2\hat{q}^2. \quad (2.4)$$

In contrast to the classical scalar observables E, q, p in (2.3) the quantum mechanical observables $\hat{H}, \hat{q}, \hat{p}$ are matrices. It is often convenient to represent the position and momentum operators in terms of the ladder operators \hat{a} and \hat{a}^\dagger as

$$\hat{q} = \frac{q_0}{\sqrt{2}}(\hat{a}^\dagger + \hat{a}), \quad \hat{p} = i\frac{p_0}{\sqrt{2}}(\hat{a}^\dagger - \hat{a}), \quad q_0 = \sqrt{\frac{\hbar}{m\omega}} \quad p_0 = \sqrt{\hbar m\omega} \quad (2.5)$$

which are expanded in the energy basis² of the oscillator. These operators act on the oscillator's energy state, a number state, by either increasing or decreasing the state's quantum occupation number n

$$\hat{a}|n\rangle = \sqrt{n}|n-1\rangle, \quad \hat{a}^\dagger|n\rangle = \sqrt{n+1}|n+1\rangle. \quad (2.6)$$

The ladder operators can be combined into *e.g.* the number operator $\hat{n} = \hat{a}^\dagger\hat{a}$. By acting on a number state, this operator counts the number of energy quanta in the state, and by this holding information of which energy eigenstate the system is in

$$\hat{n}|n\rangle = n|n\rangle. \quad (2.7)$$

When expressing the Hamiltonian in (2.4) by the operators in (2.6) and (2.7), its number basis representation is

$$\hat{H}_0 = \hbar\omega\hat{n} + \frac{\hbar\omega}{2}. \quad (2.8)$$

The first term is simply the number operator, counting the energy quanta. The second term is the zero point energy, or quantum vacuum energy. This term represents the jitter motion of the oscillator when it is in its ground state as mentioned in chapter 1. The quantum oscillator will never be "still", but fluctuate in both position and momentum. The constant term is often neglected in studies of levels above the ground state, which will also be done here. Figure 2.2

²The energy basis of the harmonic oscillator has a lot of names: number basis, occupation basis or Fock basis.

a) shows the harmonic potential and the first six quantized energy levels of the quantum harmonic oscillator. For each energy level the position wave function $\psi_n(q) = \langle q|n\rangle$ is included, to visualise the probabilistic properties of the oscillator being at some given position.

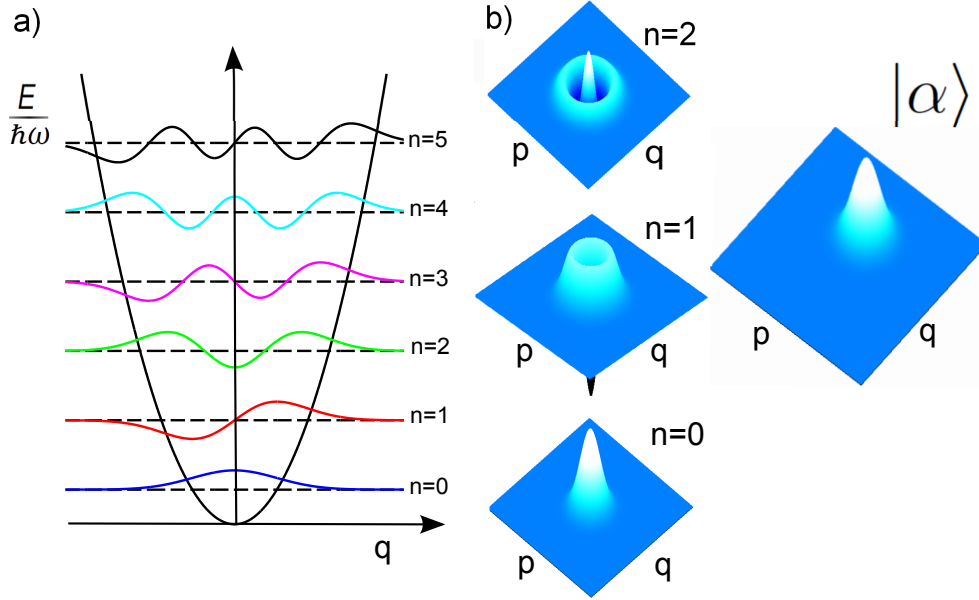


Figure 2.2: a) Quantized energy levels of the quantum harmonic oscillator with corresponding position wave functions $\psi_n(q)$ for the first six energy levels. b) Wigner representation of the first three number states of the harmonic oscillator in the phase space of (q, p) . Bottom $n = 0$, middle $n = 1$, top $n = 2$. c) Wigner representation of the coherent state ($|\alpha = 1\rangle$) in the phase space of (q, p) .

In order to draw a quantum analogy to the classical harmonic pendulum described above, the coherent state

$$|\alpha\rangle = \hat{D}(\alpha)|0\rangle = e^{-|\alpha|^2/2} \sum_{n=0}^{\infty} \frac{\alpha^n}{\sqrt{n!}} |n\rangle \quad (2.9)$$

can be introduced. This is a minimum uncertainty state which is the quantum analogue to displacing a pendulum. In (2.9) the displacement is represented in terms of the displacement operator $\hat{D}(\alpha) = \exp[\alpha\hat{a}^\dagger - \alpha^*\hat{a}]$, and the rightmost expression in (2.9) is the coherent state expanded in the number basis. When projected onto the position or momentum basis, in both bases, the coherent state wave function obtains the shape of a Gaussian wave packet with minimum uncertainty in the position and momentum observables. By (2.1) it can be shown that the time evolution of $|\alpha\rangle$ in a harmonic potential is given by

$$|\alpha(t)\rangle = \hat{U}(t)|\alpha\rangle = e^{-i\hat{H}t/\hbar}|\alpha\rangle = |\alpha e^{-i\omega t}\rangle, \quad (2.10)$$

where $\hat{H} = \hat{H}_0$ is the Hamiltonian in (2.4), t is time, and the operator $\hat{U}(t)$ is called the time evolution operator.

Quantum states in phase space of (q, p) can be conveniently visualized in terms of the Wigner distribution or the Wigner function [45, 4], which accounts for the Heisenberg's uncertainty principle. The Wigner function is a generalization of the classical phase space probability density. When applied to a quantum state, the distribution is based on the position and momentum eigenvalues, and can have negative domains³ due to interference effects of the quantum probability amplitudes. Detailed information on the Wigner function can be found in Appendix A. The Gaussian bell of the coherent state Wigner function is shown in the main figure 2.2 b) and the three lowest number states of the harmonic oscillator are shown as insets 2.2 b).

Now the pieces can be put together to represent the quantum analogy of the oscillator evolving in a harmonic potential, where its quantum state is represented by the Wigner distribution. The schematic evolution is shown in figure 2.3.

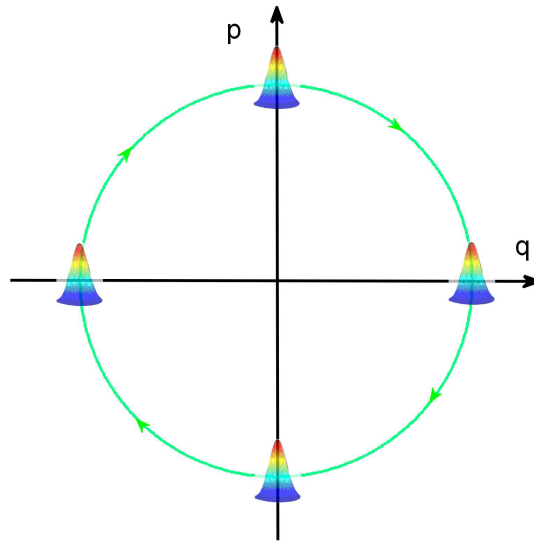


Figure 2.3: Schematic representation of the free, harmonic quantum evolution of a coherent state $|\alpha = 1\rangle$. The state is visualized by the Wigner function in the phase space of (q, p) in which it takes the form of a Gaussian wave packet, or the Gaussian bell. Contrary to the classical evolution, at every point of the trajectory, there is now an uncertainty in q and p encoded in the width of the Gaussian bell.

³The negative domains are purely quantum mechanical, with no classical analogue.

2.1.2 The Duffing Oscillator

The harmonic oscillator is in many cases an idealized model of a system. Most physical systems are nonlinear to some extent. A Duffing oscillator is widely used as a representative model in description of mechanical resonators with nonlinear elastic behaviour, like *e.g.* graphene in chapter 1. In contrast to the harmonic oscillator the anharmonic oscillator can have amplitude dependent frequency, as there is a nonlinear relation between the applied force and system response.

The total energy of the classical Duffing oscillator is given by

$$E = \frac{p^2}{2m} + \frac{1}{2}m\omega^2q^2 + \frac{\alpha_0}{4}q^4, \quad (2.11)$$

where the variables are as in equation (2.3), and α_0 is the Duffing constant. For most NEMS the Duffing part of the Hamiltonian is much smaller than the harmonic part, which is assumed here. When displacing the Duffing oscillator, in the same manner as the harmonic oscillator, it will swing back and forth about its equilibrium. The phase space trajectory will be slightly elliptic, but is hard to distinguish from the harmonic circular path without an extensive zoom.

While a quantum harmonic oscillator displays a behaviour analogous to its classical counterpart, the same does not hold for nonlinear Duffing oscillator. The presence of the nonlinearity facilitates the creation of non-classical states. In the quantum analogy, the Hamilton operator is given in terms of position and momentum operators and has an additional quartic Duffing potential term

$$\hat{H} = \frac{\hat{p}^2}{2m} + \frac{1}{2}m\omega^2\hat{q}^2 + \frac{\alpha_0}{4}\hat{q}^4. \quad (2.12)$$

Like for the harmonic oscillator, the Duffing Hamiltonian can be expressed in terms of number operators: when only keeping the ladder operator combinations with equal number of \hat{a} and \hat{a}^\dagger in \hat{q}^4 , *i.e.* performing the rotating wave approximation (RWA), which is valid when the oscillator amplitude is of the order of the zero point amplitude and $\hbar\alpha_0/m^2\omega^2 \ll \omega$, the Hamiltonian (2.12) is in number basis given by

$$\hat{H} = \hbar\omega\hat{n} + \hbar\mu\hat{n}^2, \quad (2.13)$$

where $\mu = 3\hbar\alpha_0/8m^2\omega^2$. Details on the RWA can be found in appendix B. The energy spectrum of the Hamiltonian in 2.13 has the same energy basis as (2.4), but the eigenenergies of the Duffing oscillator are slightly shifted with respect to the energy levels of the harmonic oscillator, $E_n = \hbar(\omega n + \mu n^2)$, and the energy levels are non-equidistant, as can be seen in figure 2.4 a).

Although $\mu \ll \omega$, when a quantum Duffing oscillator is initiated in a coherent state, its free evolution possesses effects which do not exist in the corresponding

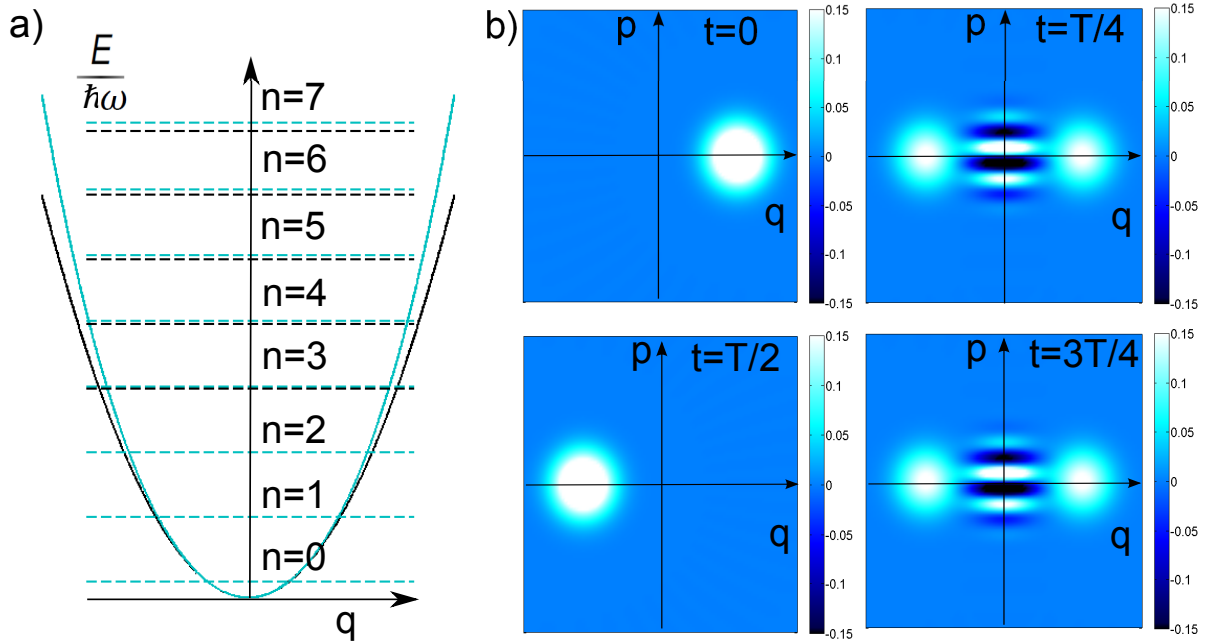


Figure 2.4: a) The first eight quantized energy levels of the Duffing oscillator with $\mu/\omega = 5 \cdot 10^{-3}$ (blue). The quantized energy levels and the potential of the harmonic oscillator are included for comparison (black). The quartic Duffing term in (2.12) shifts the energy levels with respect to the levels of the harmonic oscillator, and the energy levels are no longer equidistant. b) Schematic representation of the free quantum evolution of a coherent state $|\alpha = 2\rangle$ in a Duffing potential, $\mu/\omega = 5 \cdot 10^{-3}$. The state is visualized by the Wigner function in the phase space of (q, p) , in which it initially takes the form of a Gaussian wave packet. Due to the Duffing potential, at times $\pi/2\mu$ and $3\pi/2\mu$ the Gaussian bell evolves into a quantum superposition state - a cat state.

classical evolution. Under the evolution of (2.13) at time $t = \pi/2\mu$, the initial coherent state $|\alpha, t = 0\rangle$ evolves into a "Schrödinger cat state" a quantum superposition of two coherent states

$$|\alpha, \pi/2\mu\rangle = \frac{e^{-i\pi/4}}{\sqrt{2}} [|\alpha\rangle + i|-\alpha\rangle]. \quad (2.14)$$

In a quantum system isolated from an environment this evolution is periodic in time. As depicted in figure 2.4 b), the oscillator state will periodically evolve to a cat state at times of $T/4$ and $3T/4$, and back into a coherent state at times of $T/2$ and T , where $T = 2\pi/\mu$. At other intermediate times the oscillator undergoes a "zoo" of states, which also appear and reappear cyclically. The intermediate states do not have neat mathematical expressions. The derivation of the coherent state evolving into a cat state can be found in Appendix C.

The cat state has a distinct Wigner function representation, a top view of which is shown in figure 2.4 b), at $t = T/2$ and $t = 3T/4$. It consists of two Gaussian bells separated by interference fringes, which have alternating positive and negative domains, indicating the state being a quantum superposition. The cat state with phase of $\pi/4$, as in (2.14), is also sometimes referred to as "the Yurke-Stoler cat" as a tribute to Yurke and Stoler [46], who contributed with the early ideas on how to create a freely propagating optical superposition state. They theoretically showed that when a coherent state propagates in a Kerr medium, a medium with a nonlinear susceptibility, it can under suitable conditions, evolve into a cat state. The Kerr self phase modulation can be modelled by the Hamiltonian in (2.13). The general term "cat state" originates from the "Schrödinger cat state" and is a concept of a great physical relevance, as such a state represents the quantum mechanical essence of state superposition and entanglement.

2.2 State Superposition and Entanglement

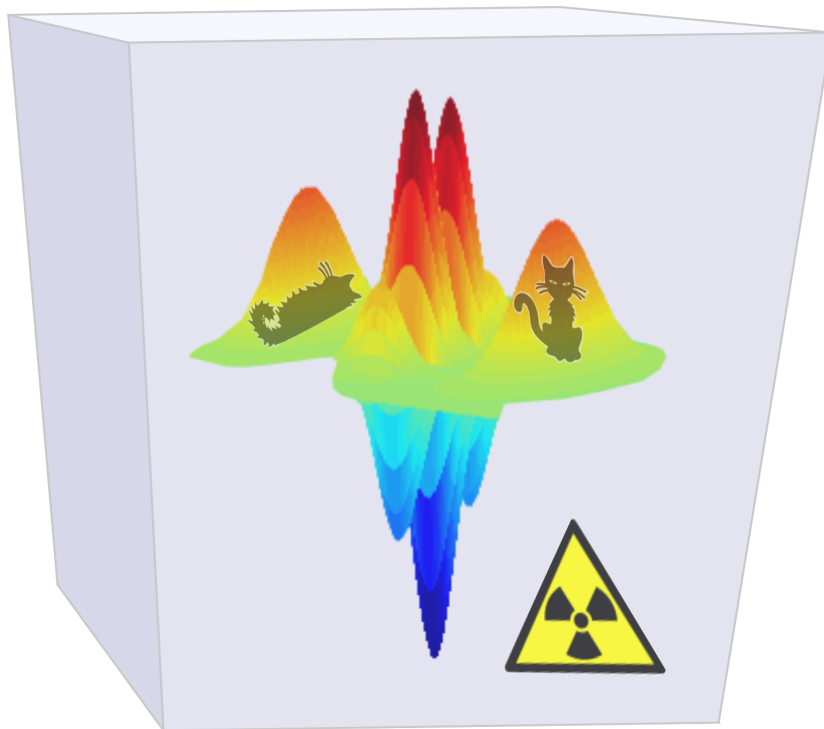


Figure 2.5: Semi-artistic interpretation of the Schrödinger's cat Gedanken experiment.

By the early 1930s the fundamental backbone of the non-relativistic quantum theoretical description of the microscopic world was established [47]. However,

the outcomes of the newly established theory showed signs of very strangely correlated behaviour in two-particle systems. Theoretical predictions of global states in spatially separated bipartite systems, which cannot be written as product states of the individual sub-systems, contradicted the common sense. Even more strangely, theoretical predictions indicated that if one sub-system were probed and resulted in a particular measurement outcome, the other sub-system would instantaneously collapse into an identical measurement outcome, or if the sub-systems were anti-correlated, the opposite outcome. It was as if the sub-systems could communicate faster than the speed of light without being directly coupled in any obvious way. This contradicted the theory of relativity.

The problem of this "spooky action at a distance" was first recognized and theoretically addressed in the historical papers of Einstein, Podolsky and Rosen (EPR) in [48], and Schrödinger in [49]. The term "entanglement" was introduced by Schrödinger as a name for the strange correlations. Although entanglement was formally accepted, it was far from understood⁴. The argument of the EPR-paper was that the existing quantum mechanical description of the physical reality was incomplete. The attempt was to use the concept of entanglement to ascribe values to physical quantities a priori to measurement by the local hidden variable model, (LHVM). This model can be comprised to three statements:

- a) Realism - measurement outcomes are properties intrinsically carried by a system, and exist prior to and independent of a measurement.
- b) Locality - measurements obtained at a certain location in space are independent of any actions performed elsewhere.
- c) Free will - the local measurement apparatus is independent and does not affect the hidden variables which determine the local measurement results.

Schrödinger on the other hand, tried to use the existing quantum formalism to explain entanglement by his famous thought experiment with the cat in a box. By this, shedding light on how one could interpret an entangled, macroscopic superposition state: The famous cat is put into a black box with a poisonous gas container. The container may by chance be broken by a mechanism triggered by the decay of a radioactive substance. An intact container means the cat is alive, which can be denoted by the system state vector $|u, a\rangle$, unbroken container, alive cat. Breaking the container results in a dead cat, denoted by the state vector $|b, d\rangle$, broken container, dead cat. After a time corresponding to many half-times of radioactive decay, and shorter than the lifetime of a cat, both outcomes are possible, but cannot be detected by the observer. Assuming the probabilities for the outcomes are equal, the system state vector can be written as

$$|\Psi\rangle = \frac{1}{\sqrt{2}} (|u, a\rangle + |b, d\rangle).$$

⁴We still do not have a complete understanding of entanglement.

The system is hence in what is called a superposition state, the so-called "cat state". Both outcomes exist simultaneously until someone performs a measurement. It is also an entangled state, since both a dead and alive cat is correlated with a broken or an unbroken container. Figure shows a semi-artistic interpretation of Schrödinger's cat Gedanken experiment.

About three decades after the initial entanglement discussion Bell theoretically proved the EPR-arguments to be wrong. In his work he showed that it is exactly the entanglement that rules out the possibility of including the classical determinism of LHV into the quantum mechanical theory [50]. Bell mathematically formalized the EPR-hypothesis. The assumptions a)-c) impose certain constraints on statistical correlations in bipartite systems and their mathematical description is referred to as the Bell inequalities. The correlations of entangled states violate the Bell inequalities, meaning that entanglement cannot be explained within the classical formalism of LHV.

The first successful experiments testing Bell's theory followed shortly after with outcomes strongly indicating entanglement's existence [51]. All doubt was removed in the following decades with numerous reports with results pointing towards the correctness of the quantum mechanical predictions [47, 52]. From the experimental reports of the past two decades it is clear that entanglement is not a merely a philosophical matter, but a quantum resource which can be manipulated, distilled, controlled, broadcast and can take on tasks that are impossible to perform classically [47]. These are strong motivation factors for continuing to extend our understanding of entangled states and their possibilities of implementation.

2.2.1 Entangled States

By general definition any pure multipartite state in the Hilbert space \mathcal{H} for a system consisting of n sub-systems

$$|\Psi\rangle \in \mathcal{H} = \otimes_{i=1}^n \mathcal{H}_i, \quad (2.15)$$

is entangled if it cannot be written as a product of n vectors corresponding to Hilbert spaces of the sub-systems \mathcal{H}_i [47]

$$|\Psi\rangle \neq |\Psi_1\rangle \otimes |\Psi_2\rangle \cdots \otimes |\Psi_n\rangle. \quad (2.16)$$

In addition to the cat states in section 2.1.2, examples of significant pure entangled states are the EPR states, also called Bell states, singlet states or e-bits⁵. These are maximally entangled states with maximal knowledge of the total system and no knowledge of the subsystems

⁵The name e-bit, entangled bit, is often used in the field of quantum information.

$$|\psi^\pm\rangle = \frac{1}{\sqrt{2}}(|0\rangle|1\rangle \pm |1\rangle|0\rangle) \quad |\phi^\pm\rangle = \frac{1}{\sqrt{2}}(|0\rangle|0\rangle \pm |1\rangle|1\rangle). \quad (2.17)$$

These states have a finite dimensional Hilbert space, consisting of finite dimensional Hilbert sub-spaces. Systems like the quantum harmonic oscillator is a continuous variable (CV) system, with a Hilbert space with an infinite dimension.

Two-mode squeezed states are entangled states of CV systems and are related to

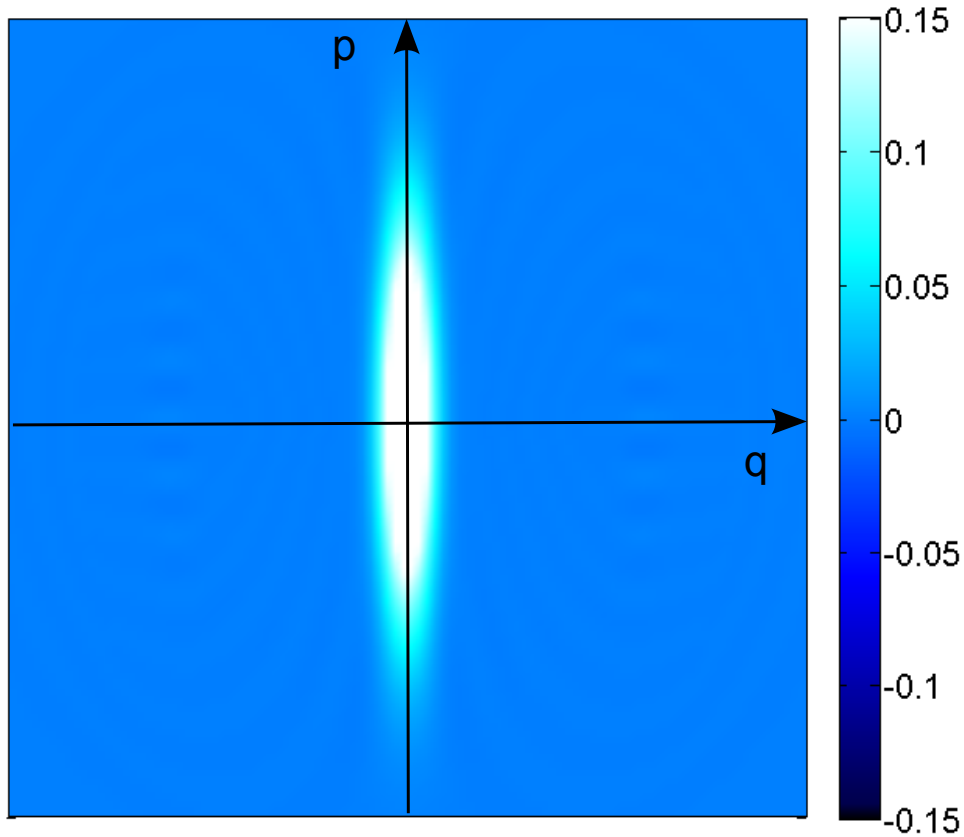


Figure 2.6: Top view of the Wigner distribution of an amplitude squeezed vacuum state with squeezing parameter $r = 1$, in phase space of position q and momentum p .

the Bell states. They are well studied, rather easily generated and implemented [17, 53]. For a single oscillator the simplest squeezed state is the squeezed vacuum state $\hat{S}|0\rangle$, where $\hat{S} = e^{\frac{1}{2}(\xi\hat{a}^2 - \xi^*\hat{a}^{\dagger 2})}$ is the squeezing operator and $\xi = re^{i\theta}$ is the squeezing parameter. The Wigner function of amplitude squeezed vacuum, in the phase space of (q, p) , is shown in figure 2.6. The Gaussian wave packet of the state is centred around the phase space origin and in contrast to the circular area of a ground state, its area is "cigar shaped". Its width is squeezed below

the minimum uncertainty in q ($r > 0$). The width of the bell is correspondingly increased in p , so the area of the state is not changed, in order not to violate the Heisenberg uncertainty relation. Correspondingly, if the squeezing is done in p ($r < 0$), the width of the Gaussian bell is increased in q .

When expanding the object of study to a bipartite system, the one-mode squeezed state can be extended to a two-mode squeezed state. The simplest is the two-mode squeezed vacuum $\hat{S}_{12}|00\rangle$, where $\hat{S}_{12} = e^{(\xi^* \hat{a}_1 \hat{a}_2 - \xi \hat{a}_1^\dagger \hat{a}_2^\dagger)}$ is the two-mode squeezing operator. Two-mode squeezed states display "Global squeezing", reduced fluctuations in linear combinations of variables of both subsystems. Individual squeezing is not observed in the fluctuations of each subsystem alone. In the limiting case of $r \rightarrow \infty$, the two-mode squeezed states approach the maximally entangled EPR states in (2.17).

All of the above mentioned states are pure entangled states. In the lab pure states are rare due to the interaction with the environment. One has to deal with mixed states, represented in terms of a density matrix $\hat{\rho}$. A mixed state $\hat{\rho}$ of n subsystems is entangled if it cannot be represented as a classical mixture of separable states

$$\hat{\rho} \neq \sum_{i=0}^{\infty} p_i \hat{\rho}_1^i \otimes \hat{\rho}_2^i \otimes \dots \hat{\rho}_n^i, \quad (2.18)$$

each with $\sum_i p_i = 1$ and $p_i \geq 0$.⁶ In order to be able to classify which states are entangled and which are not, and if entangled, how strong the entanglement is, there are developed theoretical density matrix analysis methods, which can be applied to mixed as well as to pure states. Next, the theoretical methods of state classification and entanglement quantification, used in the appended papers, will be introduced.

2.2.2 Classification and Quantification of Entanglement

One of the strongest criteria classifying whether a state is entangled or not is the Peres criterion of separability, which is shown to be true for all $2 \otimes 2$ and $2 \otimes 3$ systems [54] and also for continuous variable systems [55, 56]. The Peres criterion, also called the Positive Partial Transpose (PPT) criterion, states that if a state $\hat{\rho} = \hat{\rho}_{AB}$ is separable, then after a partial transpose

$$\langle n_A, i_B | \hat{\rho}^{\text{TA}} | m_A, j_B \rangle = \langle m_A, i_B | \hat{\rho} | n_A, j_B \rangle, \quad (2.19)$$

the eigenspectrum of $\hat{\rho}$ is still positive. If at least one eigenvalue is negative, then the state is non-separable, and by definition of (2.18), is entangled.

There exist numerous mixed state entanglement quantification methods [47, 57].

⁶A convex combination of product states.

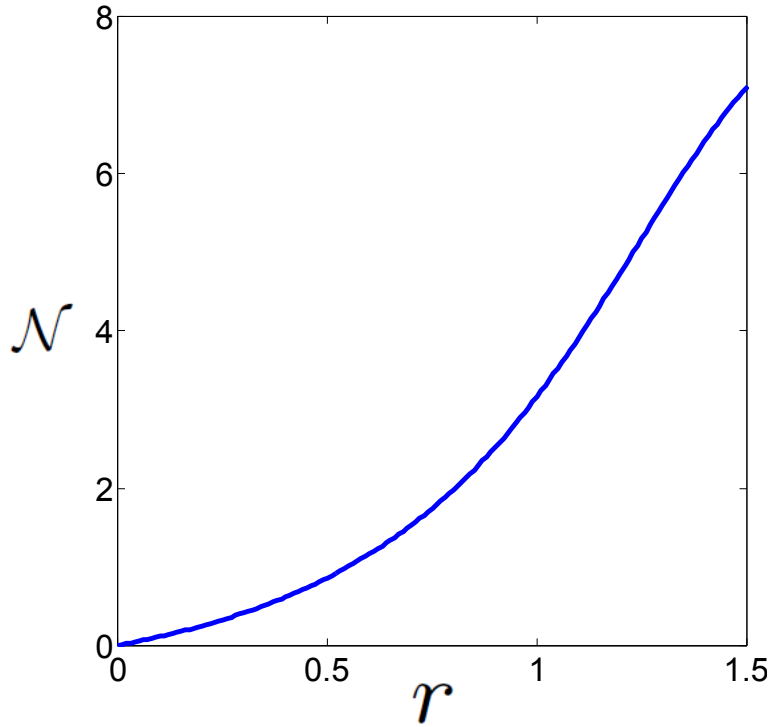


Figure 2.7: Negativity \mathcal{N} of the two-mode squeezed vacuum state as function of the squeezing parameter r .

A frequently used analytic tool is the negativity. The measure of negativity was introduced by Vidal and Werner and is built upon the PPT criterion [58]. The negativity $\mathcal{N}(\hat{\rho})$ is the sum of negative eigenvalues ε_i of the partial transpose $\hat{\rho}^{\text{TA}}$ of a density matrix $\hat{\rho} = \hat{\rho}_{\text{AB}}$, and by this measures the degree of how much ρ^{TA} fails to be positive definite

$$\mathcal{N}(\hat{\rho}) = \sum_i |\varepsilon_i|, \quad \varepsilon_i < 0. \quad (2.20)$$

An equivalent representation is

$$\mathcal{N}(\hat{\rho}) = \frac{1}{2}(\|\hat{\rho}^{\text{TA}}\| - 1), \quad (2.21)$$

where $\|\hat{\rho}^{\text{TA}}\|$ is the trace norm of the partial transpose $\hat{\rho}^{\text{TA}}$. The trace norm of any general, Hermitian operator is $\|\hat{O}\| = \text{Tr}\sqrt{\hat{O}^\dagger\hat{O}} = \sum_i \varepsilon_i$. Since $\hat{\rho}^{\text{TA}}$ may have negative eigenvalues, the general trace norm reads as

$$\|\hat{\rho}^{\text{TA}}\| = 1 + 2 \sum_i |\varepsilon_i| \equiv 1 + 2\mathcal{N}, \quad \varepsilon_i < 0. \quad (2.22)$$

Figure 2.7 shows the negativity \mathcal{N} of the two-mode squeezed vacuum state as function of the squeezing parameter r . The negativity is calculated by the method

described above. When $r = 0$ also $\mathcal{N} = 0$, and negativity's increase with r corresponds to increased entanglement of the squeezed state.

As already mentioned, an environment interaction strongly affects pure quantum states. In the next chapter this will be further discussed in the context of dissipation mechanisms.

In the previous chapter the dissipation free evolution of a harmonic and a Duffing oscillator was reviewed. In nature dissipation free systems are as good as impossible, as no system is completely isolated from interactions with its surroundings. Dissipation, or damping, refers to the transfer and conversion of energy and is an essential mechanism in physical, chemical and biological processes. In this chapter the phenomenological classical dissipative model of Brownian motion is briefly presented. The corresponding quantum description in the weak coupling limit, and how the dissipation affects the quantum states, are discussed for the cases of linear and nonlinear system-bath coupling.

3.1 Classical Dissipation

The classical model of Brownian motion, or a Wiener process¹ considers the dynamics of a particle in a viscous medium. The effects of the dissipation are treated statistically, where the influence of the environment is separated into two forces: a friction force and a random force. The classical dynamics of the dissipative system is described by the Langevin equation, which is used in a wide range of systems like particles in liquids or gases, electric circuits, motion of diatomic molecules in a solution and more. For a harmonic oscillator, linearly coupled to an environment the Langevin equation can be solved exactly.

Assume the system of interest is a harmonic or a Duffing oscillator, and couple it bilinearly to an environment which can be described by a collection of non-interacting harmonic oscillators.² The total Hamiltonian of the one-dimensional oscillator, in a potential $U(q)$, is

¹The first reports on Brownian motion came already in 1700's, but bear the name of the botanist R. Brown, who in 1827, discovered that tiny pollen grains suspended in water, exhibited a continuous but also erratic motion. This physical behaviour was explained by A. Einstein [59], showing that the particles were randomly bombarded by the water molecules. The rigorous mathematical formalization of the Brownian motion as a random process was developed out by N. Wiener. Therefore, the Brownian process is also known as the Wiener process.

²In physics this kind of environment is often called a bosonic heat bath.

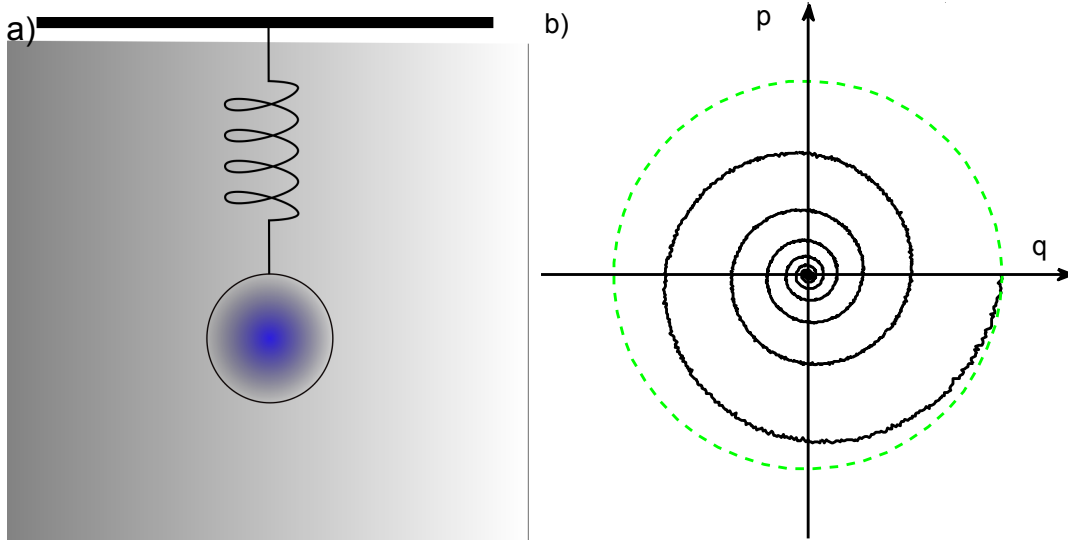


Figure 3.1: a) Schematic representation of an oscillator system immersed into a heat bath of a liquid or a gas. The oscillator interacts with the bath and is affected by the random collisions with the particles in the bath. b) Example of the classical Brownian dynamics of a harmonic oscillator in the phase space of position and momentum (q, p) . The friction and the random forces are respectively manifested in the spiral trajectory of diminishing system energy, and the random fluctuations in the trajectory line. The dashed circle is included for comparison and represents the undamped evolution of the harmonic oscillator.

$$H = \frac{p^2}{2m} + U(q) + q \sum_k g_k q_k + \sum_k \frac{p_k^2}{2m_k} + \frac{m_k \omega_k^2}{2}, \quad (3.1)$$

where p_k, ω_k, m_k are the momentum, frequency and mass of the k 'th bath mode and g_k is the coupling constant of the system's position coordinate q to the k 'th mode's position coordinate q_k . A schematic representation of the system and the bath is shown in figure 3.1 a). By means of Hamilton's equations one can from (3.1) derive the generalized Langevin equation of motion

$$m\ddot{q} = -\partial_q \tilde{U}(q) - \int_0^t d\tau \dot{q}(\tau) \Gamma(t - \tau) + R(t). \quad (3.2)$$

The terms, from left to right, are the resultant force, the restoring force from the renormalized potential $\tilde{U}(q)$, the friction force described by a memory integral containing the friction kernel $\Gamma(t - \tau)$, and a random force $R(t)$. In general, from the moment the coupling between the system and the bath is established, the friction integral depends on the entire history of the system's evolution. The physical meaning of the bath memory is the bath requiring a certain finite time to respond to any fluctuation in the system. This again affects how the bath acts

back on the system. It is often adequate to ascribe the environment an ability of memoryless response to changes. Such environment is called Markovian³, in case of which the friction kernel is $\Gamma(t) = 2\Gamma_0\delta(t)$ and the memory integral in (3.2) is easily evaluated. The special case of the Brownian motion in a Markovian environment is described by the classical Langevin equation

$$m\ddot{q} = -\partial_q\tilde{U}(q) - 2\Gamma_0\dot{q} + R(t). \quad (3.3)$$

The random force $R(t)$ is completely determined by the dynamics of the bath. For a large number of bath degrees of freedom one is simply not able to account for the detailed microscopic dynamics. It is therefore convenient to treat the bath as a macroscopic ensemble with certain statistical properties. For a harmonic bath model $R(t)$ is a Gaussian random process, called δ -correlated white noise with infinitely short correlation time $\langle R(t)R(t') \rangle \sim \delta(t - t')$. The random and friction forces are connected by the fluctuation-dissipation theorem.

For a harmonic potential $U(q) = m\omega^2q^2/2$, the Langevin equation (3.3) is often represented in the form

$$\ddot{q} + \gamma\dot{q} + \omega^2q = f(t), \quad (3.4)$$

where the renormalized quantities are $\gamma = 2\Gamma_0/m$, $f(t) = R(t)/m$. Figure 3.1 b) shows the Brownian dynamics of a harmonic oscillator in the phase space of position and momentum (q, p) , interacting with a harmonic environment. The friction force is manifested in the spiral shaped trajectory of diminishing oscillator energy, and the random force manifests itself in the fluctuations of the trajectory line. The dashed circular trajectory is included for comparison of the dissipation free evolution of the harmonic oscillator in figure 2.1 a).

3.2 Quantum Dissipation

The quantum mechanical evolution of a system interacting with an environment is given by a Quantum Master Equation (QME), the common effect of which is the irreversible relaxation to equilibrium. A quantum description of the Brownian motion is treated by several models, depending on certain approximation limits of the system in question. In the limit of weak coupling and the bath's correlation time being much smaller than the system's relaxation time, known as "the quantum optical limit", the Born-Markov QME in the RWA is a convenient description for the dissipative quantum dynamics, and is widely used [60].

The derivation of a QME begins with the von Neumann equation

³A Markov process is a random process in which the future is independent of the past, given the present.

$$i\hbar \frac{d\hat{\rho}}{dt} = [\hat{H}, \hat{\rho}], \quad (3.5)$$

which is equivalent to the Schrödinger equation (2.1), extended to consider the evolution of the total density matrix $\hat{\rho}$ of the system and the bath. The total Hamiltonian \hat{H} for the combined system consists of three terms

$$\hat{H} = \hat{H}_S + \hat{H}_{SB} + \hat{H}_B, \quad (3.6)$$

which represent the system Hamiltonian, the system-bath interaction, and the bath Hamiltonian. In the next section, the QMEs for the linear and nonlinear system-bath couplings will be discussed for the harmonic and Duffing oscillator systems. A rigorous treatment of quantum master equations can be found in the literature [60, 61].

3.2.1 Linear Coupling

The quantum Hamiltonian corresponding to (3.1) is

$$\hat{H} = \frac{\hat{p}^2}{2m} + U(\hat{q}) + \hat{q} \sum_k g_k \hat{q}_k + \sum_k \frac{\hat{p}_k^2}{2m_k} + \frac{m_k \omega_k^2 \hat{q}_k^2}{2}, \quad (3.7)$$

where the considered potential

$$U(\hat{q}) = \frac{1}{2} m \omega^2 \hat{q}^2 + \frac{\alpha_0}{4} \hat{q}^4 \quad (3.8)$$

is either the Duffing, or if $\alpha_0 = 0$, the harmonic potential. In accordance with (3.6), the first two terms on the right hand side in (3.7) represent the system Hamiltonian \hat{H}_S , the middle term is the interaction Hamiltonian \hat{H}_{SB} with a bilinear system-bath coupling, and the last term is the Hamiltonian of the bosonic bath \hat{H}_B . Inserting the Hamiltonian (3.1) into (3.5) and assuming the bath being in thermal equilibrium, Markovian, and with a weak system-bath coupling $g_k \ll \omega$ (Born approximation), the bath will not be affected by the changes in the system. The reservoir is then treated as a statistical ensemble. This enables tracing over the bath degrees of freedom, and the QME reduces to the evolution of the reduced density matrix for the system, $\hat{\rho}_S$. For the system given above, the Born-Markov QME in Schrödinger picture and RWA is

$$\dot{\hat{\rho}}_S = -i[\hat{H}'_S, \hat{\rho}_S] - \frac{\gamma(\omega)}{2} [\{\hat{a}^\dagger \hat{a}, \hat{\rho}_S\} - 2\hat{a} \hat{\rho}_S \hat{a}^\dagger] - \frac{\gamma(-\omega)}{2} [\{\hat{a} \hat{a}^\dagger, \hat{\rho}_S\} - 2\hat{a}^\dagger \hat{\rho}_S \hat{a}], \quad (3.9)$$

where $m = 1$ and $\hbar = 1$, and \hat{H}'_S is the RWA system Hamiltonian. A detailed derivation of (3.9) can be found in Appendix D. In (3.9) the first commutator term is the coherent evolution of the oscillator systems discussed in chapter 2. The term multiplied by the dissipation rate $\gamma(\omega) = \Gamma_0(N_B(\omega) + 1)$ describes the emission of energy quanta from the system to the bath. The term multiplied

by the excitation rate $\gamma(-\omega) = \Gamma_0 N_B(\omega)$ describes the absorption of the energy quanta by the system from the bath. The influence and characteristics of the bath are incorporated into the calculation of the rates, which both depend on the dissipation strength Γ_0 and the Bose-Einstein distribution $N_B(\omega)$.⁴ The excitation and dissipation terms have the same Lindblad structure [60, 62]

$$\hat{\mathcal{L}}[\hat{X}]\hat{\rho} = \{\hat{X}^\dagger \hat{X}, \hat{\rho}\} - 2\hat{X}^\dagger \hat{\rho} \hat{X}. \quad (3.10)$$

Here \mathcal{L} is the Lindblad superoperator, \hat{X} and $\hat{\rho}$ are a general operator and a density matrix. In the case of a linear system-bath coupling, \hat{X} and (\hat{X}^\dagger) are the creation and (annihilation) operators to the first power. The anti-commutator term in (3.10) governs the exponential evolution, whereas the term with operators on both sides of $\hat{\rho}$ is the jumping term, providing discrete transitions of single energy quanta.

Equation (3.9) can further be written in a compact form

$$\frac{d\hat{\rho}_S}{dt} = \mathcal{L}\hat{\rho}_S = (\mathcal{L}_0 + \mathcal{L}_1)\hat{\rho}_S, \quad (3.11)$$

with $\mathcal{L}_0\rho_S = -i[\hat{H}_S, \hat{\rho}_S]$ and $\mathcal{L}_1\hat{\rho}_S = (\mathcal{L}[\hat{a}] + \mathcal{L}[\hat{a}^\dagger])\hat{\rho}_S$. In analogy with the time evolution operator in (2.10), given that \hat{H} , and hence, \mathcal{L} are time independent, the time evolution of $\hat{\rho}_S(t)$ is

$$\hat{\rho}_S(t) = \exp[\mathcal{L}(t - t_0)]\hat{\rho}_S(t_0), \quad (3.12)$$

where $\exp[\mathcal{L}(t - t_0)]$ is the time evolution superoperator. Figure 3.2 a) shows the dissipative quantum evolution of an initial coherent state of a harmonic oscillator, $\alpha_0 = 0$ in (3.8), at temperature $T = 0$, linearly coupled to a bosonic environment. This is a quantum analogy of the classical, dissipative evolution in figure 3.1 b). The evolution is obtained by integration of the QME (3.11), and is represented by the Wigner function in the phase space of (q, p) . The leftmost dashed circle is the contour of the initial coherent state wave packet with the fluctuations incorporated into its width. The spiral is its midpoint trajectory towards the steady state. The equilibrium steady state is the ground state $|0\rangle$, centred about the origin and shown by the Wigner function (colourmap).

Figure 3.2 b) shows the dissipative quantum evolution of an initial Yurke-Stoler cat state of a harmonic oscillator at $T = 0$, linearly coupled to a bosonic environment. The evolution is represented by a Wigner function (colourmap) in the phase space of (q, p) . The four snapshots show the initial cat state at $t = 0$, decohering cat states at two subsequent times of $t = T_0$ and $t = 2T_0$, and the final equilibrium steady state, the ground state at $t = 10T_0$. Here $T_0 = 2\pi/\omega$ is

⁴The dissipation strength Γ_0 is obtained by the assumption of an Ohmic bath of non-interacting bosonic modes, which are distributed according to the Bose-Einstein distribution $N(\omega)$.

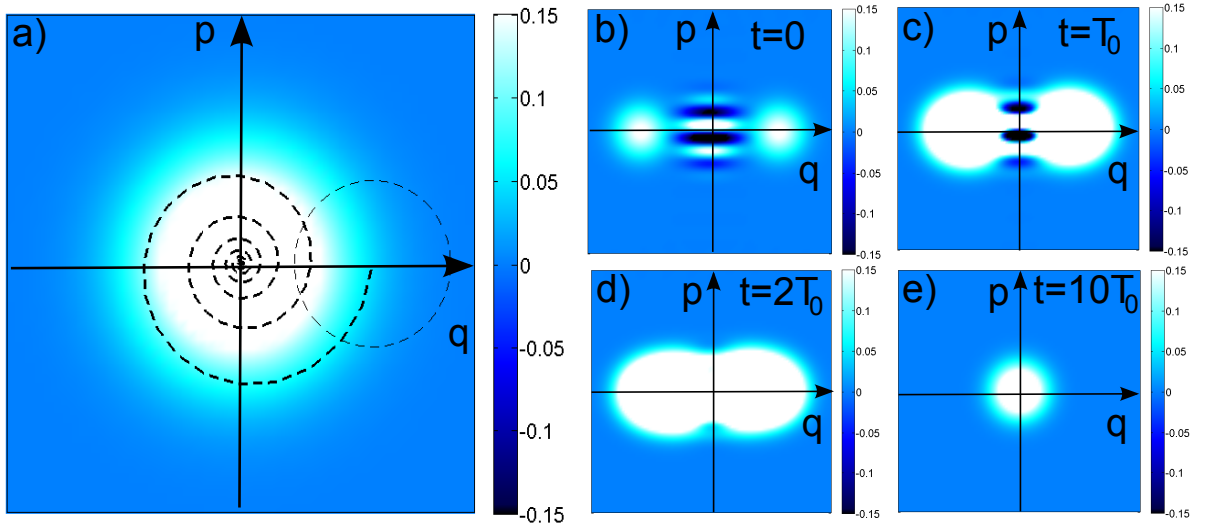


Figure 3.2: a) Dissipative quantum evolution, Wigner function representation, of a coherent state of a harmonic oscillator weakly coupled to a bosonic, Markovian environment at zero temperature. The initial state is indicated by the dashed, leftmost circular contour. The spiral indicates the trajectory of the Gaussian bell's midpoint. The Gaussian bell of the equilibrium state $|0\rangle$ is centred about the origin and is shown by the coluormap. b)- e) Dissipative quantum evolution, Wigner function representation of a Yurke-Stoler cat state with $\alpha = 2$ of a harmonic oscillator. The snap shots are taken at times $t = 0$, $t = T_0$, $t = 2T_0$, and $t = 10T_0$, where $T_0 = 2\pi/\omega$ is one period of the coherent oscillation. The cat state quickly decoheres and reaches the ground state equilibrium.

one period of the harmonic oscillation. The purpose of the figure is to visualise the quantum state's fragility and its rapid loss of quantum coherence due to the bath interaction. In the Wigner distribution of a cat state the decoherence is manifested in the loss of the interference pattern as the state evolves into a classical mixture. Finally the two Gaussian bells merge into one and center about the origin in the ground state. This behaviour has been extensively investigated and it is shown that when expressed in the coherent basis, both the diagonal and off-diagonal density matrix elements of the cat state rapidly decay. Additionally, the decoherence rate increases with the initial size of the cat [63, 64, 65].

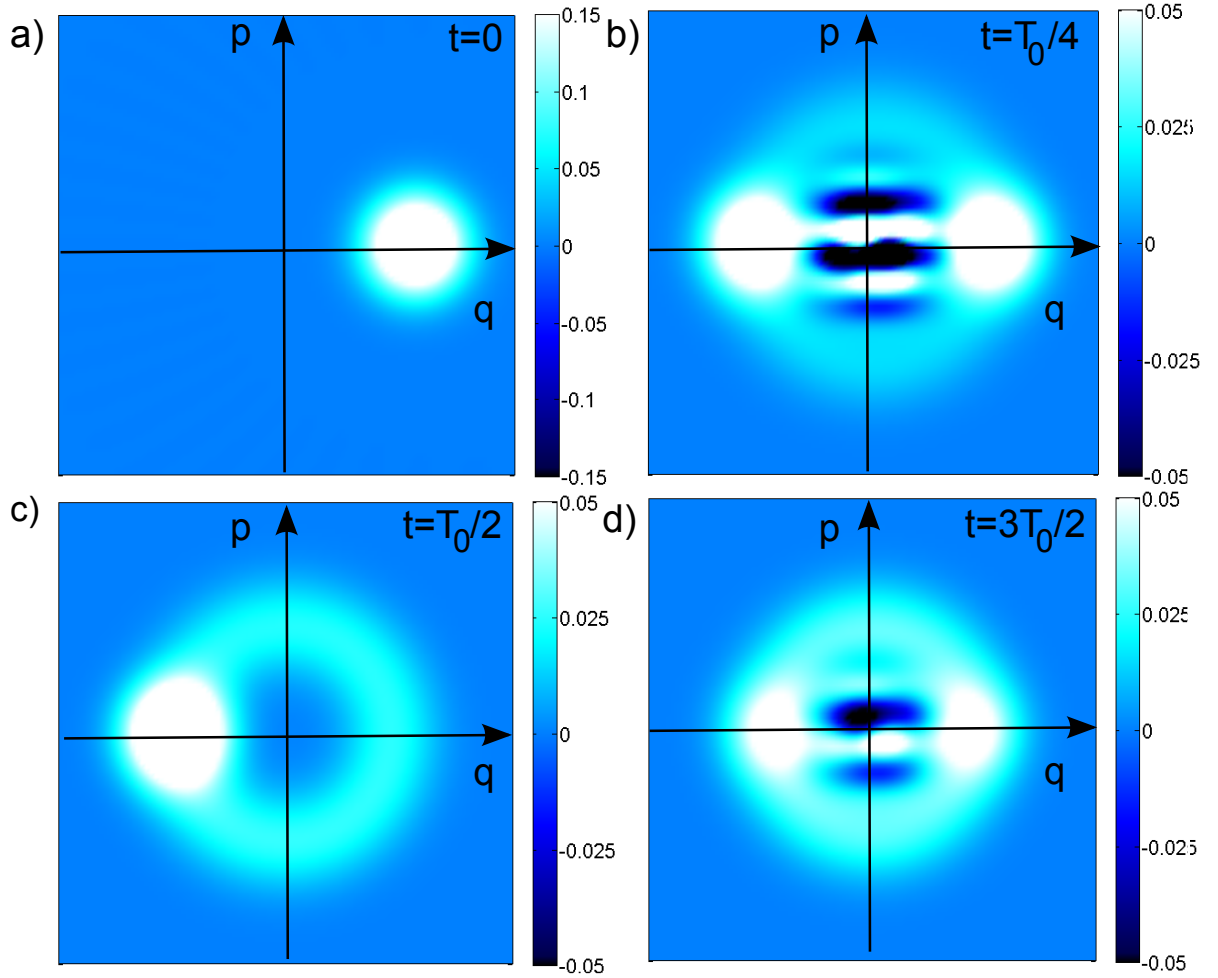


Figure 3.3: Evolution of the Wigner function of a coherent state of a Duffing oscillator, linearly and weakly coupled to a bosonic, Markovian environment at zero temperature. The snapshots are taken at times when cat states and coherent states are expected to emerge. a) Initial coherent state $|\alpha = 2\rangle$ at $t = 0$. b) The first emerging and decohering cat state at $t = T_0/4$. c) Decohering coherent state at $t = T_0/2$. d) The second, strongly decohered cat state at $t = 3T_0/4$. Here $T_0 = 2\pi/\mu$ and μ is the Duffing constant in (2.13) with $\mu/\omega = 5 \cdot 10^{-3}$.

Figure 3.3 a) - d) show the Wigner function evolution of a damped Duffing oscillator initiated with a coherent state $|\alpha = 2\rangle$. The snapshots are taken at times $t = [0, T_0/4, T_0/2, 3T_0/4]$, with $T_0 = 2\pi/\mu$, and are a comparison to the dissipation free evolution in figure 2.4 b). As in the dissipation free dynamics, the coherent evolution part of the QME (3.9) will cyclically evolve the initial coherent state into a cat state. However, this evolution is disturbed by the influence of the system-bath interaction. The effect is, as for the damped harmonic oscillator, destruction of quantum interference, prevention of state recurrence and finally, a saturation to the ground state [66].

3.2.2 Nonlinear Coupling

As seen in previous section, the linear system-bath coupling results in a dissipative process, linear damping (LD), which kills quantum coherence and relaxes the system to an equilibrium steady state. At zero temperature this is the ground state. If a system possesses conservative nonlinearities, it is natural to take into account higher orders of the system-environment coupling [67]. This results in a dissipative process, nonlinear damping (NLD), very much different from the LD. The total system Hamiltonian of an oscillator nonlinearly coupled to the environment is

$$\hat{H} = \frac{\hat{p}^2}{2m} + U(\hat{q}) + \hat{q}^2 \sum_k g_k \hat{q}_k + \sum_k \frac{\hat{p}_k^2}{2m_k} + \frac{m_k \omega_k^2 \hat{q}_k^2}{2}, \quad (3.13)$$

where the potential is as in (3.8). Compared to (3.7) the interaction between the system and the bath is now quadratic in \hat{q} , and this coupling contributes to a renormalisation of the Duffing constant, which is assumed to be negligibly small. By similar treatment as in section 3.2.1, the nonlinear QME in RWA and Schrödinger picture is

$$\dot{\hat{\rho}}_S = -i[\hat{H}'_S, \hat{\rho}_S] - \frac{\gamma(2\omega)}{2} [\{\hat{a}^{\dagger 2} \hat{a}^2, \hat{\rho}_S\} - 2\hat{a}^2 \hat{\rho}_S \hat{a}^{\dagger 2}] - \frac{\gamma(-2\omega)}{2} [\{\hat{a}^2 \hat{a}^{\dagger 2}, \hat{\rho}_S\} - 2\hat{a}^{\dagger 2} \hat{\rho}_S \hat{a}^2], \quad (3.14)$$

where H'_S is the system Hamiltonian in RWA. In analogy to (3.9) the first commutator term is the coherent evolution of the oscillator system discussed in chapter 2. The dissipative part has the Lindblad structure of equation (3.10). In current QME \hat{X} , (\hat{X}^\dagger) are creation and annihilation operators to the second power, meaning that in the case of a nonlinear system-bath coupling the discrete energy transitions involve two quanta. As in (3.9) the term multiplied by the dissipation rate $\gamma(2\omega) = \Gamma_0(N_B(2\omega) + 1)$ describes the emission of two energy quanta from the system to the bath. The term multiplied by the excitation rate $\gamma(-2\omega) = \Gamma_0 N_B(2\omega)$ describes the absorption of two energy quanta by the system from the bath. The influence and characteristics of the bath are incorporated into the calculation of these rates. Both depend on the dissipation strength Γ_0 and the Bose-Einstein distribution $N_B(2\omega)$. The detailed derivation of (3.14) can be found in Appendix D.

The two-quanta transition process provides parity conservation of the initial quantum state's density matrix elements. This results in a non-classical steady state, which at $T = 0$, is a coherent superposition of the ground and the first excited number states [68]

$$\hat{\rho}_S(t = \infty) = \rho_{00}|0\rangle\langle 0| + \rho_{01}|0\rangle\langle 1| + \rho_{10}|1\rangle\langle 0| + \rho_{11}|1\rangle\langle 1|. \quad (3.15)$$

This can be shown, as by the QME in (3.14), $\dot{\hat{\rho}}_S(t = \infty) = 0$. The NLD-preserved coherence of the off-diagonal matrix elements is a contrast to linear damping, by

which ρ_{01} and ρ_{10} would rapidly vanish. This can be inferred by the QME in (3.9), by which $\hat{\rho}_S(t = \infty) \neq 0$.

Figure 3.4 a) shows the Wigner distribution of the initial state $|\alpha = 1\rangle$ of a harmonic oscillator, and b) shows the steady state, described by (3.15), in which the oscillator saturates. The negative domain in the Wigner distribution confirms the steady state's non-classical features. A further discussion of the NLD and its effects on quantum states of single and bipartite oscillator systems, at both $T = 0$ and $T > 0$, will be presented in chapter 4.

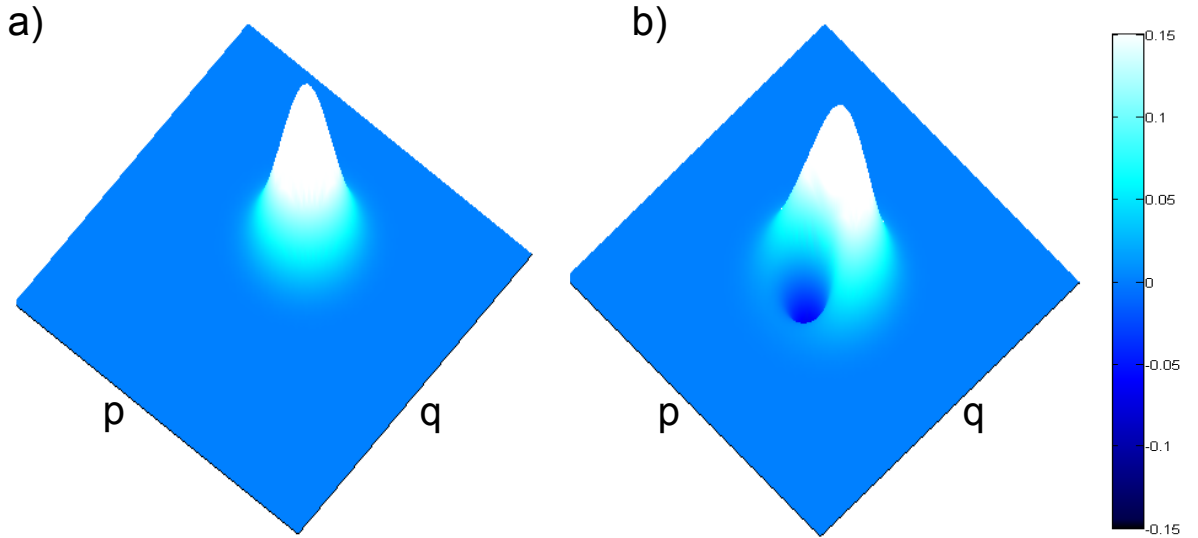


Figure 3.4: a) Wigner function of the initial coherent state of harmonic oscillator $|\alpha = 1\rangle$. b) Wigner function of the non-classical steady state of the harmonic oscillator, as result of the nonlinear system-bath coupling to a bosonic, Markovian environment at zero temperature. The dark, negative domain in the Wigner distribution indicates the state's non-classicality.

CHAPTER 4

Summary of Appended Papers

This chapter serves as a summary of the appended papers put into the context of the previous chapters. In paper I the main question of interest is what kind of quantum features can be observed in the dynamics of the two lowest degenerate vibrational modes of a nonlinear graphene resonator. The system consisting of a graphene membrane and two voltage back-gates is isolated from the interaction with the environment and the mode dynamics is analysed. In paper II the Duffing oscillator system investigated in paper I is extended to include environment interaction. The focus is directed towards the dynamics of the lowest vibrational mode. The main interest lies within what kind of quantum features emerge when the system-bath interaction is nonlinear, and how these properties are further influenced by inclusion of linear damping. The following paper III extends the analysis in paper II to a bipartite system of two coupled Duffing oscillators, each nonlinearly interacting with an environment. The primary quest is how the NLD influences the entanglement of initially separable states in such a system. Paper IV is a continuation of paper III in which the study is extended to initially entangled states. The asymptotic entanglement is investigated in the parameter space of squeezing, dissipation rate and temperature. This is done for two different bath configurations. The study also includes a systematic comparison with known results of asymptotic entanglement in linearly damped bipartite systems.

4.1 Paper I

Generating Macroscopic Superposition States in Nanomechanical Graphene Resonators

In this paper the system consisting of a graphene membrane, suspended over two voltage gates is investigated. The system is assumed to be in the quantum regime and isolated from interactions with the environment. Figure 4.1 shows the system setup of the square graphene membrane suspended above two local backgates. By manipulating the membrane with voltage pulses, generation of non-classical Schrödinger cat states in the membrane's lowest flexural modes is possible. For a comparative convenience with the appended paper, the notation here will be as in the original manuscript. For detailed description of equations

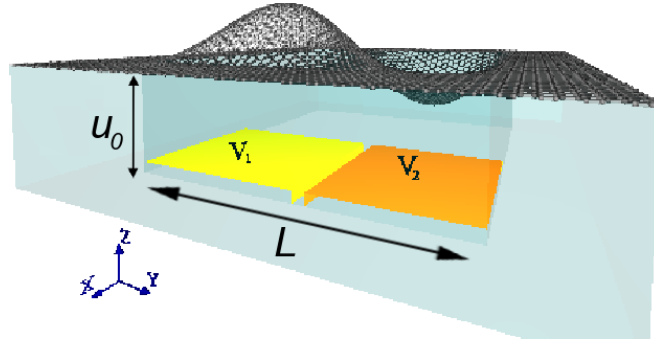


Figure 4.1: Cross section of a square graphene membrane resonator. A fully clamped graphene membrane with side L is suspended a distance u_0 above the substrate. Below, covering two adjacent quadrants beneath the membrane, are local backgates with time dependent voltage biases $V_{1,2}(t)$. By applying pulses to the local gates, non-classical states can be generated.

and parameters, please see publication I.

The graphene sheet behaves as a nonlinear membrane, and the attention is restricted to its two lowest degenerate deflection modes. These modes are quantized and labelled as mode **1** and mode **2**. When both modes are initially in the ground state $|0, 0\rangle$ and a common bias pulse is applied to both gates at time $t > 0$, the system of the two flexural modes is described as two weakly interacting quantum Duffing oscillators, where oscillator **2** is displaced. For details see equation (6), paper I. The displacement of mode **2** arises from the voltage dependent capacitive coupling between the membrane and the gate. The dynamics of the modes decouple as their coupling term is shown to be weak, and during the voltage onset mode **1** remains close to its ground state. By focusing on mode **2**, introducing the displaced ladder operator basis transformation $\hat{b}_2 = \hat{a}_2 - \xi_0/\sqrt{2}$, and applying RWA, the system Hamiltonian of mode **2** resembles the Yurke-Stoler Hamiltonian (2.13) discussed in chapter 2. The initial ground state of mode **2** in the a -basis corresponds to a coherent state in the displaced b -basis $|0\rangle_{a_2} = |-\xi_0/\sqrt{2}\rangle_{b_2}$ at the instant of the voltage onset. Figure 4.2 a) and b) schematically illustrate the system before and at the instant of the voltage pulse. In 4.2 a) the Gaussian wave packet centred about the origin represents the position probability distribution $P(\xi)$ of the amplitudes ξ of mode **2**. The mode is in the ground state $|0\rangle_{a_2}$ of a Duffing potential in the original coordinate system of the a -basis.

When the voltage is on, the potential of mode **2** is displaced with ξ_0 and lowered with respect to the origin of the a -basis, as shown by the parabola in figure 4.2 b). The potential energy of the wave packet increases with respect to the bottom of the potential well. The b -basis represents a coordinate system which is shifted with respect to the a -basis coordinate system. Here the origin corresponds to

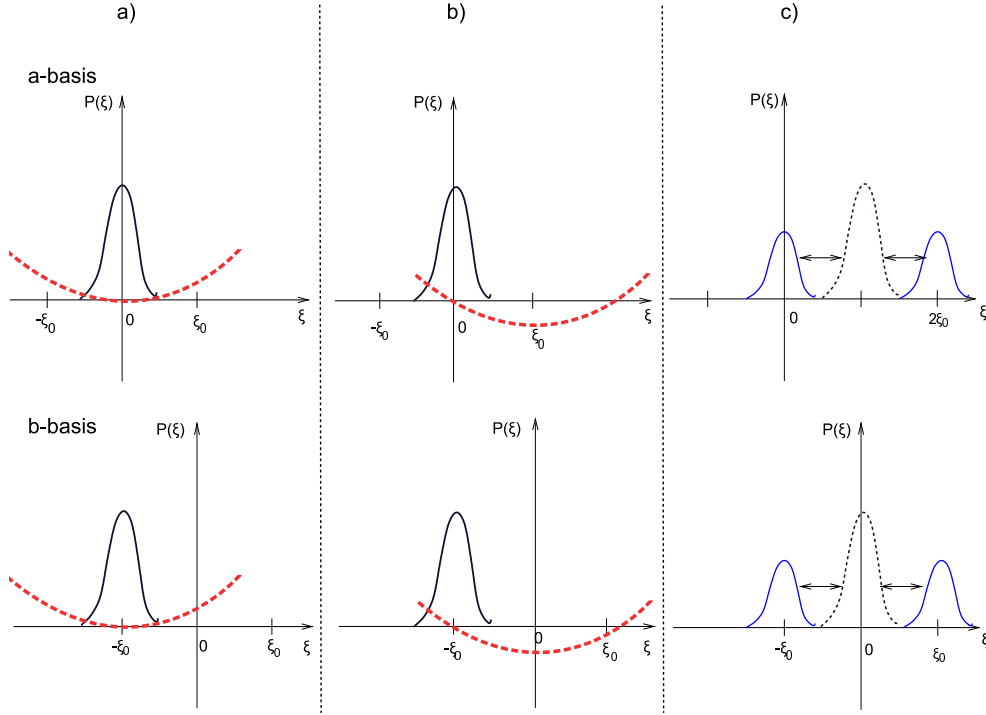


Figure 4.2: Schematic representation of the Gaussian probability distribution $P(\xi)$ of the mode amplitude ξ , represented in two coordinate systems (a and b -bases) for three different cases: a) Probability distribution in the case of no gate voltage. The potential is represented by the parabola. b) Probability distribution at the instant of the voltage onset. c) Probability distribution at the instant of the superposition states (4.1). The arrows in c) represent the motion of the wave packets.

the a -basis coordinate ξ_0 , so that at the instant of the voltage onset the potential well is symmetric about the origin in the b -basis, and the state of the wave packet is the coherent state $|\xi_0/\sqrt{2}\rangle_{b_2}$. This is shown in the lower part of figure 4.2 b).

In agreement with the discussion in section 2.1.2 in chapter 2, the coherent state evolved by the Hamiltonian (2.13), should transform into an interaction picture cat state in the b -basis

$$|\psi(T_1)\rangle = \frac{1}{\sqrt{2}} [e^{-i\pi/4} |-\xi_0/\sqrt{2}\rangle_{b_2} + e^{i\pi/4} |\xi_0/\sqrt{2}\rangle_{b_2}], \quad (4.1)$$

$$= \frac{1}{\sqrt{2}} [|0\rangle_{a_2} + i|\sqrt{2}\xi_0\rangle_{a_2}]. \quad (4.2)$$

at time $T_1 = \pi/2\mu$, where μ is the Duffing constant. Or equivalently, to an overall phase, the state in (4.1) can be transformed to the interaction picture cat state in the a -basis (4.2). The state superposition obtained in (4.1) and (4.2) can be interpreted as the mode having two equally probable amplitudes, with their

Gaussian distributions centred at coordinates 0 and $2\xi_0$ in the a -basis. The b -basis represents the same properties, only in a shifted coordinate system, where the wave packets are centred at the distance $|\xi_0|$ on both sides of the origin. This is displayed in figure 4.2 c). The arrows indicate the movement of the wave packets and the dashed wave packet is included for comparison with figure 4.2 b).

In figure 4.3 a) the numerical time evolution of the position probability density

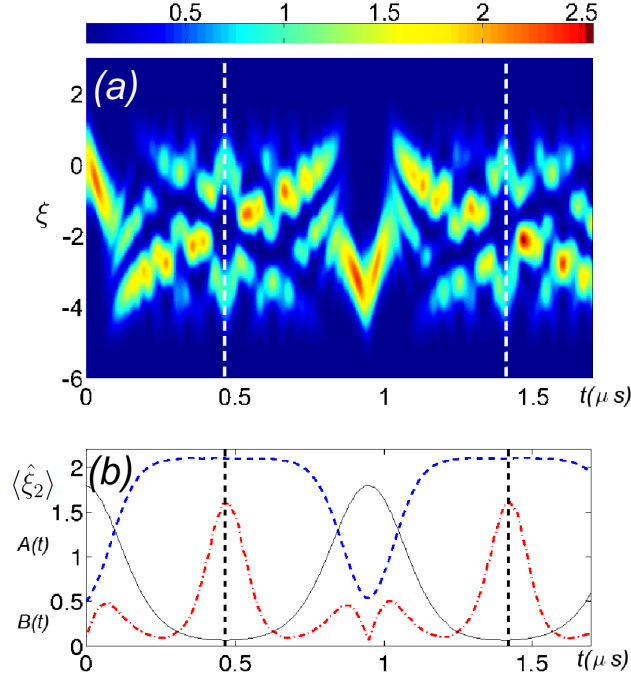


Figure 4.3: a) Snapshots of numerical time evolution of the position probability distribution of mode **2**. The snapshots are taken at the turning points of the corresponding classical trajectory of the system. The the positions (y-axis) are scaled to the quantum zero point fluctuations. b) Corresponding time evolution of the envelopes of $\langle \hat{\xi}_2 \rangle$ and its associated quantum fluctuations $\langle \Delta \hat{\xi}_2^2 \rangle \sim A(t) + B(t) \cos(2\omega t)$; The appearance of a cat state is signalled by a decrease in $\langle \hat{\xi}_2 \rangle$ along with an increased $\langle \Delta \hat{\xi}_2^2 \rangle$ in the noise of $\langle \hat{\xi}_2 \rangle$. Vertical dashed lines indicate the agreement with (a).

of mode **2** is shown. The dashed lines indicate the emerging cat states. A signature of the cat state is a reduction of the average position expectation value $\langle \hat{\xi}_2 \rangle$ together with an increase of its quantum fluctuations $\langle \Delta \hat{\xi}_2^2 \rangle$. This is shown in figure 4.3 b) where the envelopes of $\langle \hat{\xi}_2 \rangle$ and $\langle \Delta \hat{\xi}_2^2 \rangle$ corresponding to figure 4.3 a), respectively decrease and increase, as the cat state emerges.

By applying voltage on one gate, even more intricate states, non-product su-

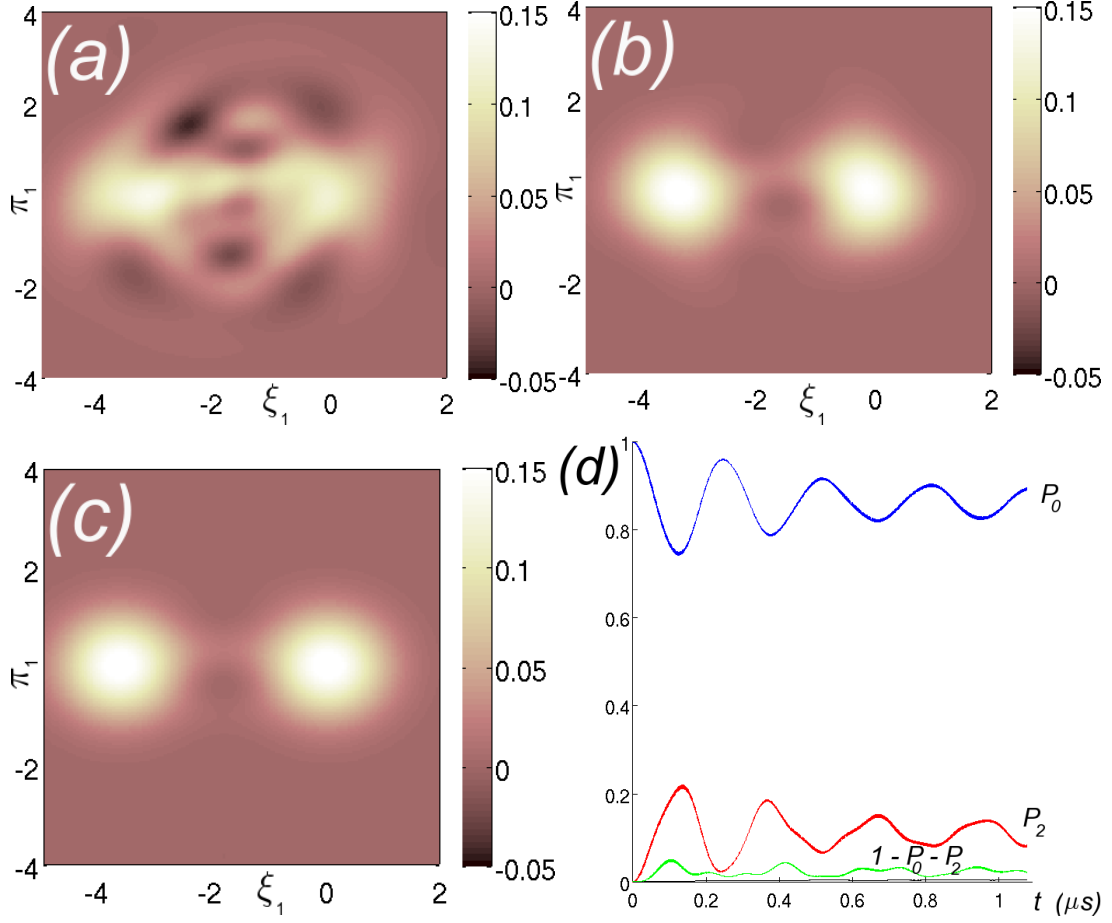


Figure 4.4: a) Top view of the reduced Wigner distribution of mode **1** in phase space of position and momentum (ξ_1, π_1) , of the numerically evolved initial state $|0, 0\rangle_a$, sampled at \tilde{T}_1 . The reduced Wigner distributions are identical for both modes, both having a bimodal structure. b) Wigner distribution of a), where $\alpha|\chi\rangle$ is removed. c) Wigner distribution of $|0, 0\rangle_a + i|-\sqrt{2}\eta_0, -\sqrt{2}\eta_0\rangle_a$. d) Time evolution of conditional probabilities of mode **1** being in the d -basis' ground, second or all other eigenstates.

perposition states, can be generated. The system Hamiltonian of the two modes with one active gate describes the dynamics of two coupled, non-degenerate and displaced Duffing oscillators. When performing a basis transformation which diagonalizes the linearly coupled modes. The Hamiltonian in the new d -basis describes two Duffing oscillators, one of them displaced, and coupled together by a quartic coupling which is stronger than the quartic coupling in the two-gate configuration. The initial ground state $|0, 0\rangle_a$ corresponds in the d -basis to

$$|0, 0\rangle_a = |0, \eta_0\rangle_d.$$

After evolution with the Duffing-like Hamiltonian in equation (11) in paper I, this state should enter a cat-like non-product state

$$|\psi(\tilde{T}_1)\rangle \propto |0, \eta_0\rangle_d + i |0, -\eta_0\rangle_d + \alpha |\chi\rangle. \quad (4.3)$$

The remainder $\alpha |\chi\rangle = \alpha \sum_{n=1} |n\rangle_{d_1} |\Psi_n\rangle_{d_2}$ is present due to the quartic coupling term in equation (11) in paper I. The numerically obtained Wigner distribution of the reduced density matrix $\hat{\rho}_1$, of mode **1** in a -basis at time \tilde{T}_1 is shown in figure 4.4 a). The distribution has a bimodal structure. The state component $|0, \eta_0\rangle_d + i |0, -\eta_0\rangle_d$ corresponds to a cat-like non-product state $|0, 0\rangle_a + i |-\sqrt{2}\eta_0, -\sqrt{2}\eta_0\rangle_a$ in a -basis. Figure 4.4 b) shows the Wigner distribution in a) after the component $\alpha |\chi\rangle$ is removed by projection. The reduced Wigner distribution of the state $|0, 0\rangle_a + i |-\sqrt{2}\eta_0, -\sqrt{2}\eta_0\rangle_a$ is included for reference in figure 4.4 (c). To ensure that the $\alpha |\chi\rangle$ component is not of major significance, the time evolution of the the conditional probabilities of mode **1** being in either its d -basis ground, second eigenstate, or all other but these two eigenstates, is shown in figure 4.4 d).

4.2 Paper II

Multi-Phonon Relaxation and Generation of Quantum States in a Nonlinear Mechanical Oscillator

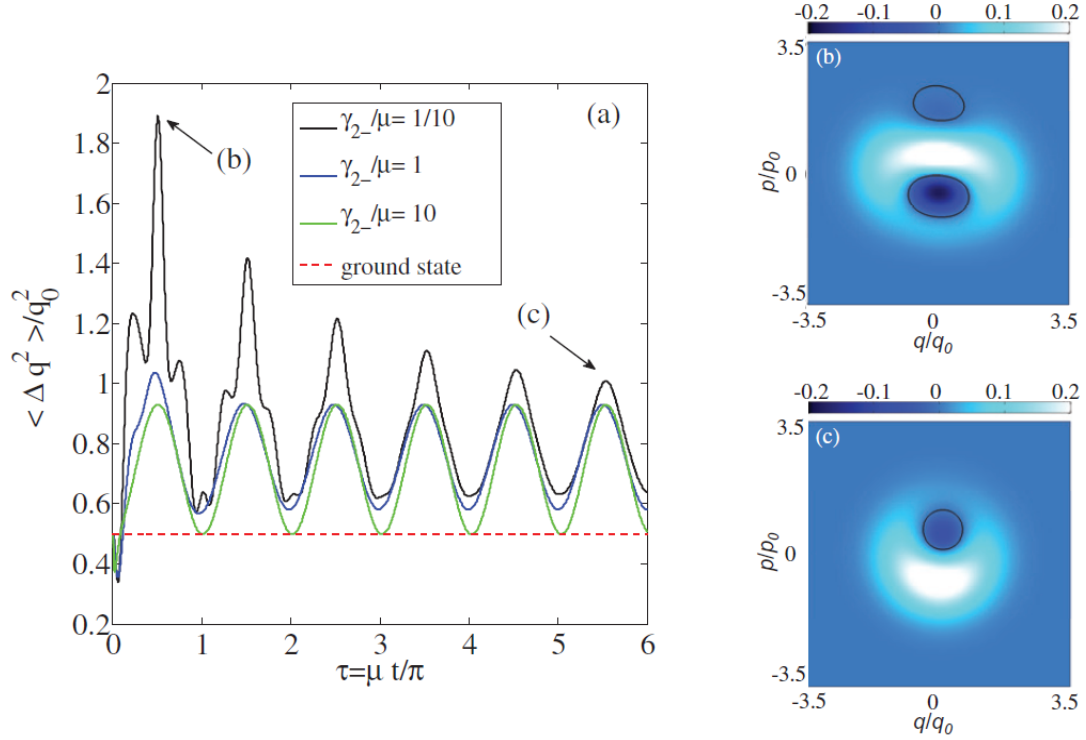


Figure 4.5: a) Nonlinear relaxation of a coherent state $|\alpha = 1\rangle$ of a Duffing oscillator via a Yurke-Stoler cat state to a non-classical steady state at $T = 0$ for three NLD rates γ_{2-} . b) Wigner distribution of the most prominent cat-like state sampled at $\tau = 1/2$. c) Wigner distribution of the non-classical steady state. The distributions in both b) and c) display negative non-classical domains. The dashed line indicates the variance of the ground state.

The study in this paper considers quantum evolution of coherent states of a Duffing oscillator mode, with the system Hamiltonian given by (3.13), subject to nonlinear dissipation (NLD). The two-quanta energy exchange with the bath is considered. Quantum features in the mode's position variance are analysed at zero and finite temperatures, opening for the possibility of state verification in a ring-down setup. The intricate interplay of LD and NLD is also investigated.

Figure 4.5 a) shows the nonlinear relaxation of the position variance of an initial coherent state of a Duffing oscillator at zero temperature for three NLD rates

γ_{2-} . For short times the Duffing part of the oscillator's Hamiltonian brings the system into a cat-like state, indicated by the significant variance increase. This is most prominent in the graph with $\gamma_{2-}/\mu = 1/10$ at $\tau = 1/2$. The Wigner distribution of this state is shown in figure 4.5 b). By letting the mode emit two energy quanta to the bath at a time, due to parity conservation, the state evolves into a non-classical steady state with a structure of the state in equation (3.15), with weights ρ_{ij} completely determined by the initial state. The Wigner distribution of the non-classical steady state is displayed in figure 4.5 c), and the state's non-zero, complex off-diagonal elements ρ_{01} and ρ_{10} cause oscillations in the position variance.

The variance of the steady state obtained by NLD depends on the oscilla-

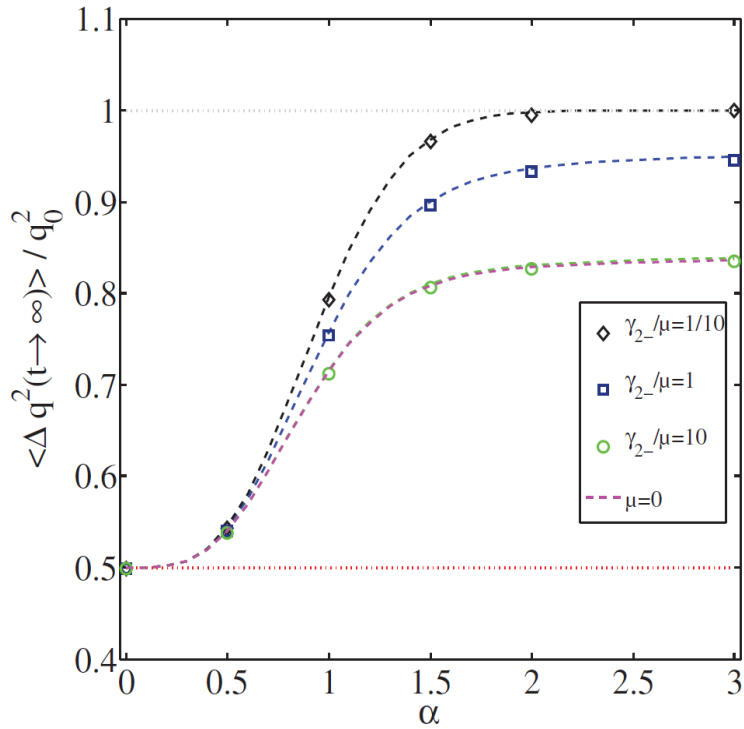


Figure 4.6: Numerical (symbols) and analytical (lines) zero temperature position variance of the NLD steady state versus initial displacement amplitude α . The variance is averaged over one period $2\pi/\mu$ and displayed for three values of NLD rate. The straight line shows the variance of the LD steady state, the ground state.

tor's initial displacement amplitude, and the ratio between the damping rate γ_{2-} and the Duffing constant μ . This is demonstrated numerically and analytically in figure 4.6. This behaviour is different from the linear decay, which always brings the system to the ground state. The variance of the ground state (straight line)

is included in figure 4.6 for comparison.

For low finite temperatures the relaxation is sequential. During the first short

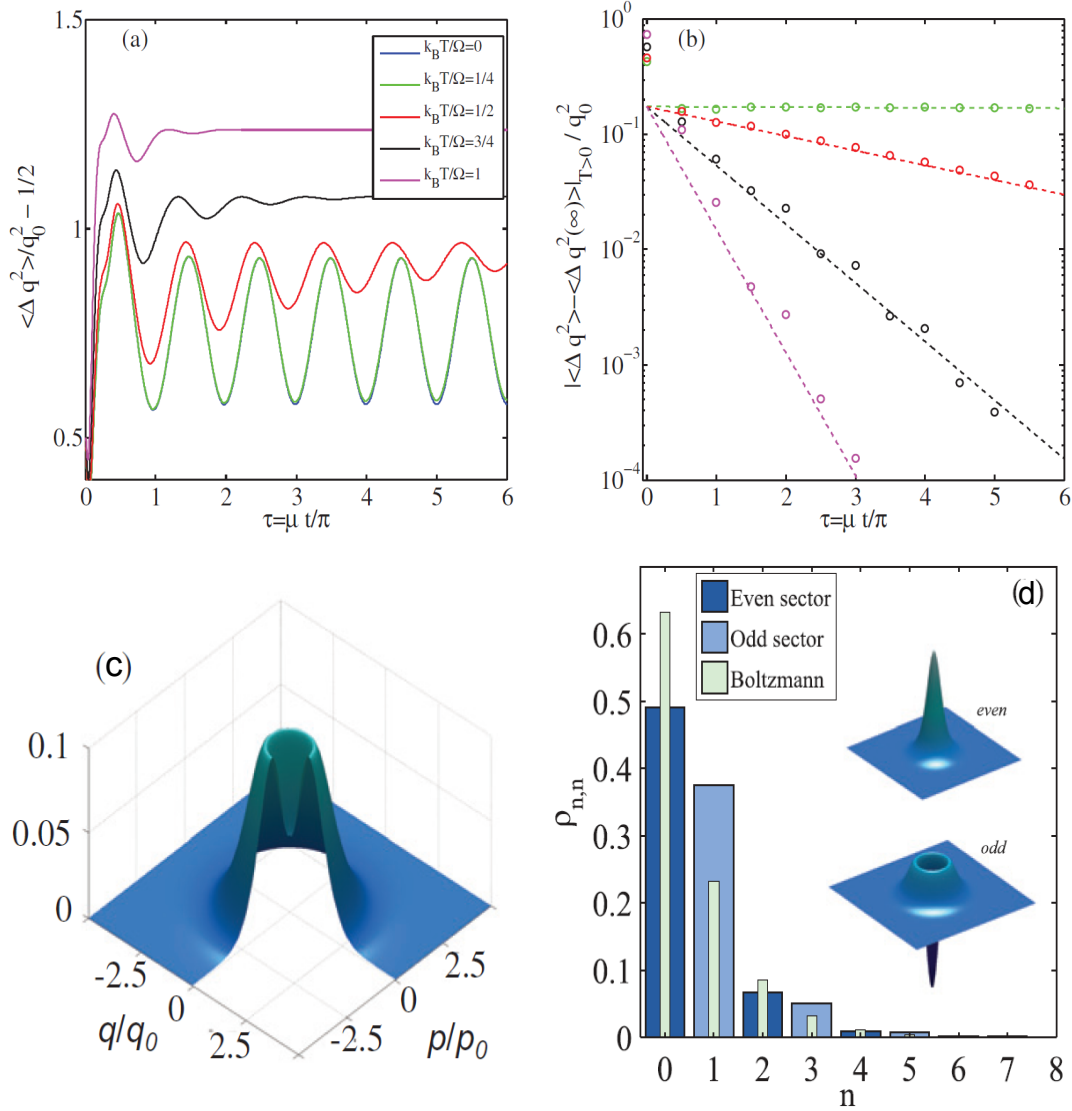


Figure 4.7: a) Nonlinear, sequential relaxation of the position variance at $T > 0$. b) Asymptotic decay of the off-diagonal density matrix elements due to bath excitations. c) Wigner distribution of the thermal steady state with $\gamma_{2-} = \mu$, $\alpha = 1$ and $k_B T / \Omega = 1$. A sector is cut out for better visualization. d) Boltzmann distribution of the even and odd parity sectors of the steady state in c). The insets show the Wigner distributions of the even and odd sectors.

time sequence of $\sim 1/\gamma_{2-}$ the NLD brings the system to the non-classical state

(3.15) with preserved coherence. During the second long sequence, the thermal two-quanta excitations contribute to destruction of the coherence. Figure 4.7 a) shows the NLD relaxation of the position variance of an initial coherent state for several finite temperatures. The variance saturates to larger values due to thermal excitations of higher energy levels. Figure 4.7 b) shows the analytical (lines) and numerical (symbols) asymptotic thermal decay of the off-diagonal density matrix elements. The thermal steady state has only diagonal density matrix elements where the even and the odd parities each are distributed according to the Boltzmann distribution. This is illustrated in figure 4.7 c) and d), where in c) the Wigner distribution of the thermal steady state is shown. The probability distribution of the even and odd number state parity sectors together with the Boltzmann distribution are displayed in figure 4.7 d).

For the interplay of the linear and nonlinear damping mechanisms the evolution is intricate. The sequential relaxation is still present. An investigation of the state decay in the second, long relaxation sequence, allows for a reconstruction of the non-classical properties of the NLD-created state during the short initial relaxation sequence.

4.3 Paper III

Nonlinear-Dissipation-Induced Entanglement of Coupled Non-linear Oscillators

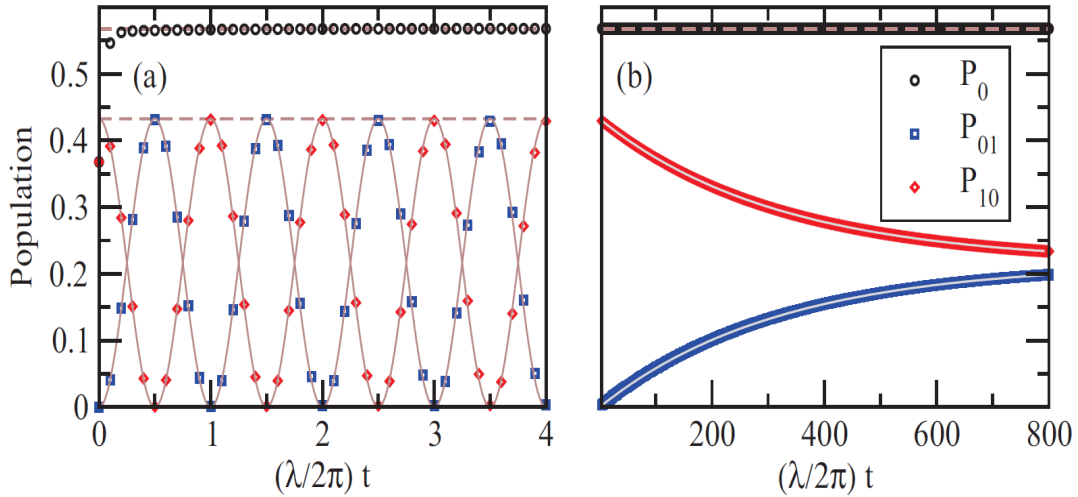


Figure 4.8: Evolution of the probability amplitudes $P_{00} = \rho_{00,00}$, $P_{01} = \rho_{01,01}$ and $P_{10} = \rho_{10,10}$ of the initial state $|\alpha_1 = 1\rangle \otimes |0\rangle$, evolved by the total Hamiltonian of two linearly coupled Duffing oscillators, nonlinearly interacting with individual reservoirs. a) Short time dynamics displaying quick saturation of the lowest state populations and oscillations between the states $|0, 1\rangle$ and $|1, 0\rangle$ due to oscillator coupling. b) Long time evolution of the envelopes of the states in a). The coupling between the oscillators contributes to a slow dephasing and decrease of oscillation amplitude of P_{01} and P_{10} . The symbols and lines represent numerical and analytic state evaluation.

The system discussed in previous paper is extended to two weakly coupled quantum Duffing oscillators, each nonlinearly coupled to an individual dissipative environment. Similarly to paper II, during the evolution the total parity is conserved. At zero temperature in the short time limit the NLD facilitates creation of a non-classical state, weights of which are determined by the initial state. In the long time limit the presence of the oscillator coupling leads to dephasing of certain density matrix elements, but also contributes to asymptotic entanglement saturation.

The initial separable state of single oscillator displacement $|\alpha_1 = 1\rangle \otimes |0\rangle$ is investigated. Figure 4.8 shows the evolution of $\rho_{00,00} = P_{\text{even}}$, $\rho_{10,10} = P_{10}$ and

$\rho_{01,01} = P_{01}$. In figure 4.8 a) the oscillating behaviour of P_{10} and P_{01} is visible in addition to the quick saturation of P_{even} due to NLD. The sum $P_{10} + P_{01} = P_{odd}$ initially saturates at a constant value. Figure 4.8 b) shows the envelopes of P_{even} , P_{10} and P_{01} in the long time limit. Due to the presence of the oscillator coupling, the amplitudes of P_{10} and P_{01} undergo a slow dephasing and gradually saturate to the same value.

The oscillator coupling creates entanglement which is quantified by the measure

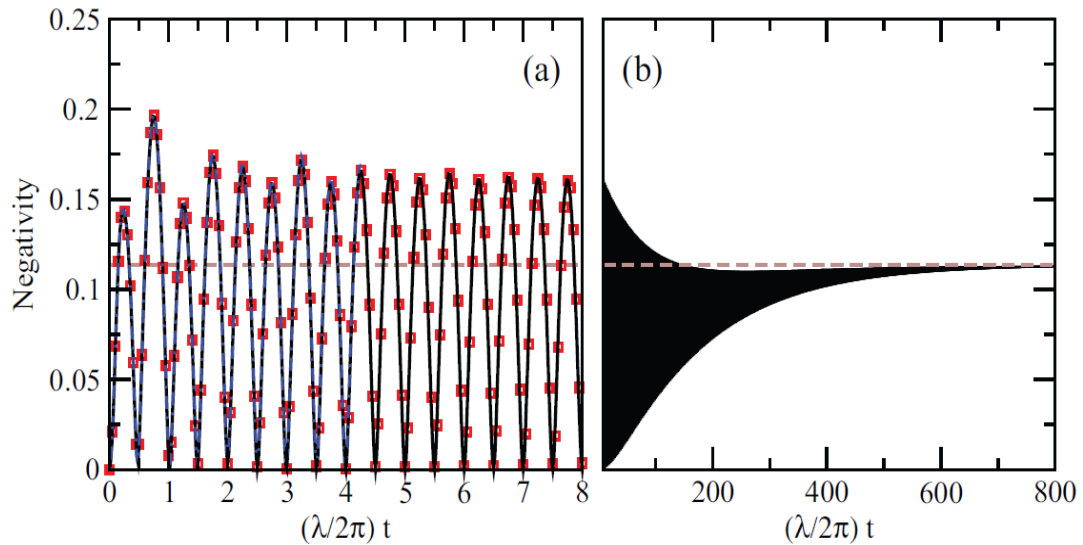


Figure 4.9: Negativity quantifying the evolving entanglement of the initial state $|\alpha_1 = 1\rangle \otimes |\alpha_2 = 0\rangle$. a) Short time negativity dynamics. b) Asymptotic negativity dynamics. The negativity is governed by $|\rho_{01,10}|^2$. The symbols and lines represent two different numerical algorithms.

of negativity, discussed in section 2.2.2. By comparing figures 4.8 a) and 4.9 a), the negativity attains maximal amplitudes when $P_{01} = P_{10}$, corresponding to maximum oscillator coherence. Minimum negativity values also appear periodically and coincide with maximum amplitudes of either P_{01} or P_{10} , corresponding to minimum oscillator coherence. It is shown that the negativity is mainly governed by the evolution of the preserved coherence matrix elements $\rho_{01,10}$ and $\rho_{10,01}$, which asymptotically saturate to a constant value. The saturation of the negativity is shown in figure 4.9 b).

The relaxation analysis is also performed for the initial state $|\alpha_1 = 1\rangle \otimes |\alpha_2 = 1\rangle$. The state's dynamics displays similar short term and asymptotic features as for single oscillator displacement. At finite temperatures signs of the entanglement

sudden disappearance and revival is seen in the negativity's evolution.

4.4 Paper IV

Entanglement Dynamics of Squeezed Vacuum States Nonlinearly Coupled to Thermal Environments

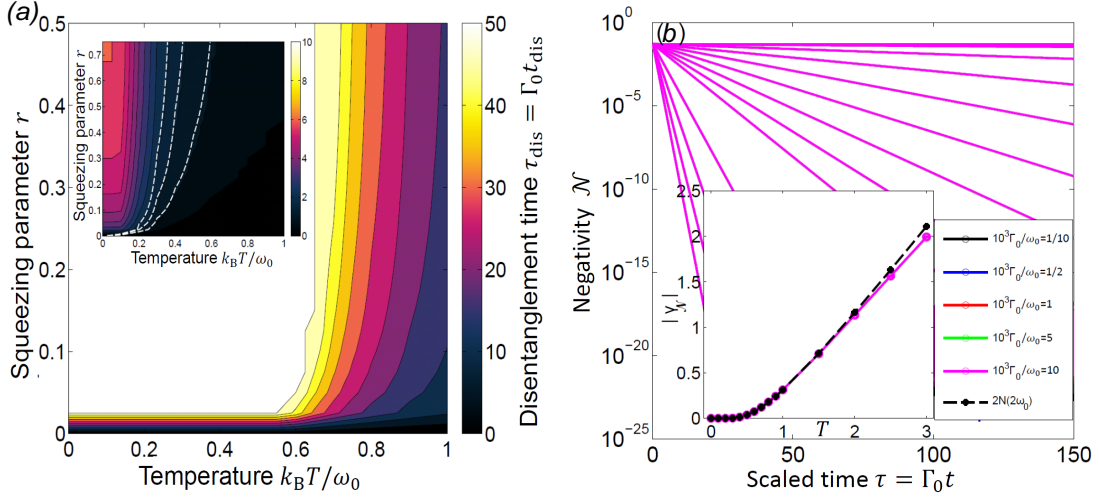


Figure 4.10: a) Main figure: disentanglement time (colourbar) of nonlinearly damped two-mode squeezed vacuum states as function of temperature and squeezing parameter for two individual baths. Inset: disentanglement time (inset colourbar scale) of linearly damped two-mode squeezed vacuum states for two individual baths, with axes and simulation parameters as in the main figure. The dashed lines are the contours of theoretically predicted disentanglement times. b) Main figure: Time evolution of the negativity of a nonlinearly damped squeezed two-mode vacuum with squeezing parameter $r = 1/20$, individual bath configuration, for several temperatures and damping rates. Inset: Slope of the negativity, $|\gamma_{\mathcal{N}}|$, extracted from the second half of the points in the main figure, as function of temperature. The dashed line is a slope fit of $2N(2\omega_0)$.

The asymptotic entanglement of two quantum harmonic oscillators nonlinearly coupled to an environment is investigated. The analysis considers configurations of one common and two individual reservoirs. The study is limited to harmonic oscillators, as in paper III it was found that the presence of a weak Duffing nonlinearity does not affect the asymptotic entanglement. In this way the isolated effect of the nonlinear system-bath coupling can be investigated. The systems are initialized with two-mode squeezed vacuum states, entanglement of

which is quantified by the negativity. The evolution of negativity is studied as function of temperature, initial squeezing and system-bath coupling strength. The results are compared with those of systems with a linear reservoir interaction.

It is known that in the case of a linear reservoir coupling the asymptotic entanglement of two-mode squeezed vacuum states depends on the bath configuration. In the case of two individual baths and uncoupled oscillators, all initial states will disentangle. This is shown in the inset of figure 4.10 a), where the disentanglement time is given as function of the squeezing parameter and temperature.

In the case of the individual bath configuration but with a nonlinear reservoir coupling, the state disentanglement is considerably slower. The disentanglement time as function of squeezing and temperature is displayed in the main figure 4.10 a). For the chosen evolution time the white region in the figure indicates that a part of the NLD states remain entangled. After a longer evolution all states will eventually disentangle. The parity conservation of NLD affects the asymptotic disentanglement. At zero temperature the initial state is evolved into a steady state with a finite negativity. For finite temperatures this state will slowly disentangle by thermal dephasing. This process is slow, as for the nonlinear coupling the thermal dephasing requires simultaneous excitation of both oscillators. Figure 4.10 b) shows the evolution of the negativity for a fixed value of r and several temperatures and dissipation strengths Γ_0 . The slope of the graphs $|\gamma_{\mathcal{N}}|$ increases with increasing temperature. The colour coded graphs with the same temperature and different Γ_0 overlap. This indicates that the decay is solely temperature dependent. The inset of figure 4.10 b) shows the extracted negativity slope as function of temperature. The fit of the slope (dashed line) is a function of the Bose-Einstein distribution, $|\gamma_{\mathcal{N}}| = 2N(2\omega_0)$, verifying the temperature dependence of the negativity decay.

For individual oscillators linearly coupled to a common bath there is a sharp transition between steady state entanglement and disentanglement in the phase space of squeezing and temperature. The persistent entanglement is connected to the relative oscillator motion degree of freedom being decoupled from the bath. For the oscillator system nonlinearly coupled to a common bath no such mode decoupling occurs, and all states disentangle in a manner very similar to the individual bath configuration shown in main figure 4.10 a) and b). The oscillators should in principle be able to exchange information via the bath, as the Lindblad superoperator does contain an information exchange term. However, for zero and low temperatures this term's effect is suppressed.

Finally, for weakly coupled oscillators, parity protection in combination with coherent oscillations in the oscillator populations, leads to disappearance and reappearance of entanglement reminiscent of ESDR behaviour.

The work presented in this thesis has evolved from analysis of a quantum system isolated from the environment to an open quantum system, where the effects of nonlinear dissipation have been investigated. Also, the system itself was extended from an individual to a bipartite system. This opened up for a study of how the system's entanglement is affected by a nonlinear interaction with a common and individual reservoirs. A general outcome is the generation of nonclassical states by the means of the Duffing nonlinearity and the nonlinear system-bath interaction.

It has been shown that the two lowest degenerate modes of a graphene membrane in quantum regime behave as weakly coupled Duffing oscillators, and can be externally manipulated by voltage pulses. By this, the modes can either be coupled or the motion of one mode can be isolated from the other. When considering the isolated one-mode case, an initial coherent state, corresponding to mode displacement, will by a free evolution transform into a Schrödinger cat state. By coupling the modes, cat-like non-product states in both modes are generated. This is possible due to graphene's onset of nonlinear response at small deflection amplitudes.

By focusing on one Duffing oscillator mode with a nonlinear coupling to the environment, displacing it and letting it evolve, the mode does not equilibrate to the ground state. Instead, due to the parity protection mechanism of the nonlinear coupling, it settles in a nonclassical steady state both at zero and finite temperatures. When considering an interplay of both linear and nonlinear decay, if the latter dominates, a sequential relaxation is observed. In the first sequence the initial state relaxes into a nonclassical state, followed by an exponential decay.

The sequential relaxation is also seen in a bipartite system of coupled Duffing oscillators, nonlinearly interacting with individual environments. The nonlinear system-bath coupling contributes to the protection of total parity, and the system settles in a nonclassical steady state. The oscillator coupling entangles initially separable states and the entanglement is preserved due to the parity conservation. Even if the coupling could be turned off at some later time, the

nonlinear damping would preserve the entanglement.

It was also found that the asymptotic entanglement of the bipartite system is not influenced by a weak Duffing nonlinearity. Therefore, when studying the asymptotic features of initially entangled states, a system of two uncoupled harmonic oscillators, nonlinearly coupled to an environment, was chosen. The environment was either a common bath or two individual baths. When comparing to a system with a linear bath interaction, the parity conservation of the nonlinear coupling reduces the disentanglement rate. There is no qualitative difference between nonlinear exchange with two individual baths or a common bath. This is in contrast to a situation with the linear coupling. When the oscillators are weakly coupled, protection of total parity in combination with single quantum exchange between the oscillators, leads to appearing and disappearing entanglement. Similar behaviour has been reported for linearly damped bipartite systems.

When reviewing the current experimental status of NEMS in quantum regime, more and more research groups are able to reach the system's lowest quantum level. Regarding the carbon based NEMS like graphene resonators, the quantum regime should be attainable. The current challenge lies within graphene's weak coupling to the readout mechanism, but the prognosis of reaching the ground state is positive. Observations of nonlinear damping have been reported in several NEMS systems in classical regime, but a scenario where the nonlinear damping rate exceeds the the linear damping rate has not yet been shown possible. Schemes on how to reach this kind of dissipative behaviour have been proposed. Two-mode squeezed states entangling a NEMS and a propagating microwave field have been realized and pave a promising route for further exploration of quantum theory in macroscopic objects and might serve as a possible future application in information processing.

CHAPTER 6

Acknowledgements

You never go through your life alone. During your journey you encounter numerous teachers, and they all offer you valuable lessons. Some lessons are easy, some are not. Although, it is often the toughest lessons which contribute to your growth and understanding of who you are and which values you support. I would therefore sincerely thank all the teachers I have encountered, for by your lessons I have grown. I would like to thank my supervisors, colleagues, my amazing friends and my family.

Thank you for your lessons.

APPENDIX A

The Wigner Function

The Wigner function can be interpreted in a following way. Consider a system with a single degree of freedom, like a particle moving in one dimension. The quantum state of the particle is described by the wave function $|\psi\rangle$, or equivalently by the operator $\hat{\rho} = |\psi\rangle\langle\psi|$. Assume the particle performs a jump from the position eigenstate $|x'\rangle$ to another position eigenstate $|x''\rangle$. The jump length is ξ and the center of the jump is denoted by $x = (x'' + x')/2$. The probability of the jump is $\langle x''|\hat{\rho}|x'\rangle$. By expressing x' and x'' in terms of the jump length and the center point, $x' = x - \xi/2$ and $x'' = x + \xi/2$, the jump probability can be rewritten as $\langle x + \xi/2|\hat{\rho}|x - \xi/2\rangle$. A distribution of the momentum p can be found by performing a Fourier transform of the $\langle x''|\hat{\rho}|x'\rangle$. From this one arrives at the definition of the Wigner Distribution

$$\mathcal{W}(x, p) = \frac{1}{2\pi\hbar} \int_{-\infty}^{\infty} d\xi e^{-ip\xi/\hbar} \langle x + \frac{\xi}{2} | \hat{\rho} | x - \frac{\xi}{2} \rangle, \quad (\text{A.1})$$

where $(2\pi\hbar)^{-1}$ is the normalization factor, ensuring that $\int \int \mathcal{W}(x, p) dx dp = 1$. The Wigner distribution is a Fourier transform of the density operator, which in position representation depends on two variables x and ξ . Transforming one of the position variables, leaves two variables in the distribution: the center of the jump, x , and the Fourier variable of the jump, p .

From the Wigner distribution the position probability distribution $\mathcal{W}(x)$ or the momentum probability distribution $\mathcal{W}(p)$ can be obtained by integration. The position distribution is found by

$$\int_{-\infty}^{\infty} dp \mathcal{W}(x, p) = \int_{-\infty}^{\infty} d\xi \langle x + \frac{\xi}{2} | \hat{\rho} | x - \frac{\xi}{2} \rangle \delta(\xi) = \langle x | \hat{\rho} | x \rangle = \mathcal{W}(x)$$

where $\delta(\xi) = \frac{1}{2\pi\hbar} \int_{-\infty}^{\infty} dp e^{-ip\xi/\hbar}$ is the Dirac-delta function. The momentum distribution can be found in a similar manner by integrating $\mathcal{W}(x, p)$ over x . The integration technique can also be used to extract the necessary information from the Wigner distribution involving several objects $W(\mathbf{x}, \mathbf{p})$, where $\mathbf{x} = [x_1, x_2, \dots, x_i]$, $\mathbf{p} = [p_1, p_2, \dots, p_i]$ and for a product state

$$W(\mathbf{x}, \mathbf{p}) = \prod_i \mathcal{W}(x_i, p_i). \quad (\text{A.2})$$

A.1 The Moyal Function

When the Wigner function is expressed in terms of the energy eigenstates of a harmonic oscillator, it is referred to as the Moyal function. The wave function can be represented in the energy occupation basis as $|\psi\rangle = \sum_n \alpha_n |n\rangle$. The density matrix is then $\hat{\rho} = |\psi\rangle\langle\psi| = \sum_{n,m} \alpha_n \alpha_m^* |n\rangle\langle m|$, and the Wigner distribution is given by

$$W(x, p) = \sum_{n,m} \alpha_n \alpha_m^* \mathcal{W}_{nm}(x, p),$$

where

$$\mathcal{W}_{nm}(x, p) = \frac{1}{2\pi\hbar} \int_{-\infty}^{\infty} d\xi e^{-ip\xi/\hbar} \langle x + \frac{\xi}{2} | n \rangle \langle m | x - \frac{\xi}{2} \rangle. \quad (\text{A.3})$$

Rewriting $\langle x + \frac{\xi}{2} | n \rangle = \psi_n(x + \frac{\xi}{2})$ and $\langle m | x - \frac{\xi}{2} \rangle = \psi_m^*(x - \frac{\xi}{2})$ in terms of the position wave functions of a harmonic oscillator $\psi_n(x)$ given in (A.7), equation (A.3) is a Fourier transform of the shifted position wave functions

$$\mathcal{W}_{nm}(x, p) = \frac{1}{2\pi\hbar} \int_{-\infty}^{\infty} d\xi e^{-ip\xi/\hbar} \psi_m^*(x - \xi/2) \psi_n(x + \xi/2).$$

It can be shown that for $n \leq m$ (A.3) attains the form

$$\mathcal{W}_{nm}(x, p) = \frac{(-1)^n}{2\pi} \sqrt{\frac{2^n n!}{2^m m!}} e^{-|X|^2} (2X)^{m-n} L_n^{m-n}(2|X|^2), \quad (\text{A.4})$$

expressed in terms of the generalized Laguerre polynomial $L_n^{m-n}(2|X|^2)$ and the phase space coordinate $X = x + ip$, where x is normalized by the spatial quantum fluctuation x_0 and p is normalized by the quantum fluctuation of momentum p_0 . For $m \leq n$, n and m interchange. Appendix A covers the calculation of $\mathcal{W}_{nm}(x, p)$.

For the n 'th energy eigenstate, $n = m$, (A.4) reduces to

$$\mathcal{W}_n(x, p) = \frac{(-1)^n}{2\pi} e^{-|X|^2} L_n(2|X|^2), \quad (\text{A.5})$$

elucidating the negative values in the Wigner distribution. The Laguerre polynomial of m 'th order has m zeros as function of $|X|^2 = x^2 + p^2$, hence $\mathcal{W}(x, p)$ oscillates between positive and negative values, as shown in figure 2.2 b). These oscillations are quantum mechanical effects, to which classical parallels cannot be drawn.

Calculation of the Moyal Function

In previous section the Moyal function of a harmonic oscillator was given by $W(x, p) = \sum_{n,m} \alpha_n \alpha_m^* \mathcal{W}(x, p)$. This section is dedicated to a detailed calculation

of

$$\mathcal{W}_{nm}(x, p) = \frac{1}{2\pi\hbar} \int_{-\infty}^{\infty} d\xi e^{-ip\xi/\hbar} \psi_m^*(x - \xi/2) \psi_n(x + \xi/2). \quad (\text{A.6})$$

The position wave functions $\psi(x)$ of a harmonic oscillator are given by

$$\psi_n(x) = (2^n n!)^{-1/2} (\pi x_0^2)^{-1/4} \exp[-(x/x_0)^2/2] H_n(x/x_0). \quad (\text{A.7})$$

Here $H_n(x)$ is a Hermite polynomial of n 'th order and x_0 is the spatial quantum fluctuation of the oscillator. Inserting (A.7) into (A.6) one obtains

$$\mathcal{W}_{nm}(x, p) = N_{nm} \int_{-\infty}^{\infty} d\xi e^{-ip\xi/\hbar} e^{-\frac{1}{2}(x+\xi/2)^2} e^{-\frac{1}{2}(x-\xi/2)^2} H_n(x + \xi/2) H_m(x - \xi/2),$$

where $N_{nm} = (2^{(n+m)} n! m! \pi x_0^2)^{-1/2} / 2\pi\hbar$ is the normalization factor. For convenience, let $x/x_0 \rightarrow x$, $p/p_0 \rightarrow p$ and set $\hbar = 1$. By the variable change $\tilde{\xi} = \xi/2 + ip$ and $Y = x - ip$ and $X = -Y^*$, the expression becomes

$$\mathcal{W}_{nm}(x, p) = N_{nm} e^{-(x^2+p^2)} \int_{-\infty}^{\infty} d\tilde{\xi} e^{-\tilde{\xi}^2} H_n(\tilde{\xi} + Y) H_m^*(-(\tilde{\xi} + X)).$$

Rewriting $H_m(-(\tilde{\xi} + X)) = (-1)^m H_m(\tilde{\xi} + X)$ gives

$$\mathcal{W}_{nm}(x, p) = (-1)^m N_{nm} e^{-(x^2+p^2)} \int_{-\infty}^{\infty} d\tilde{\xi} e^{-\tilde{\xi}^2} H_n(\tilde{\xi} + Y) H_m(\tilde{\xi} + X).$$

Further use the identities $H_n(a+b) = \sum_k^n \binom{n}{k} H_k(a) (2b)^{n-k}$ and $\int_{-\infty}^{\infty} dx e^{-x^2} H_l(x) H_k(x) = \delta_{kl} 2^k k! \sqrt{\pi}$ to subsequently obtain

$$\begin{aligned} \mathcal{W}_{nm} &= (-1)^m N_{nm} e^{-(x^2+p^2)} \sum_{k=0}^n \sum_{l=0}^m \binom{n}{k} \binom{m}{l} (2Y)^{n-k} (2X)^{m-l} \int_{-\infty}^{\infty} d\tilde{\xi} e^{-\tilde{\xi}^2} H_k(\tilde{\xi}) H_l(\tilde{\xi}) \\ &= \frac{(-1)^m}{2\pi} \frac{e^{-(x^2+p^2)}}{\sqrt{2^{(n+m)} n! m!}} \sum_{k=0}^{\min(n,m)} \binom{n}{k} \binom{m}{k} (2X)^{m-k} (-2X^*)^{n-k} 2^k k!. \end{aligned}$$

The expression above can now be rewritten in terms of the Laguerre polynomials.

By rewriting the index one gets for $n \leq m$

$$\begin{aligned} \mathcal{W}_{nm} &= \frac{(-1)^m}{2\pi} \frac{e^{-(x^2+p^2)}}{\sqrt{2^{(n+m)} n! m!}} \left(\frac{2^n}{2^n}\right) \sum_{k=0}^n \binom{n}{k} \binom{m}{k} (2X)^{m-k+n-n} (-2X^*)^{n-k} \left(\frac{1}{2}\right)^{-k} k! \\ \mathcal{W}_{nm} &= \frac{(-1)^m}{2\pi} \frac{e^{-(x^2+p^2)}}{\sqrt{2^{(n+m)} n! m!}} 2^n (2X)^{m-n} \sum_{k=0}^n \binom{n}{k} \binom{m}{k} (2X)^{n-k} (-2X^*)^{n-k} \left(\frac{1}{2}\right)^{n-k} k! \end{aligned}$$

It can be shown that

$$\begin{aligned} \sum_{k=0}^n \binom{n}{k} \binom{m}{k} (2X)^{n-k} (-2X^*)^{n-k} \left(\frac{1}{2}\right)^{n-k} k! &= \\ \sum_{k=0}^n \binom{n}{k} \binom{m}{k} (-4|X|^2)^{n-k} \left(\frac{1}{2}\right)^{n-k} k! &= n! L_n^{m-n}(2|X|^2) \end{aligned} \quad (\text{A.8})$$

And the final expression reads

$$\mathcal{W}_{nm} = \frac{(-1)^n}{2\pi} \sqrt{\frac{2^n n!}{2^m m!}} e^{-|X|^2} (2X)^{m-n} L_n^{m-n}(2|X|^2). \quad (\text{A.9})$$

Here $L_n^{m-n}(2|X|^2)$ is the generalized Laguerre polynomial. For $m \leq n$ the index n and m is interchanged.

Validation of (A.8)

$$S = \sum_{k=0}^n \binom{n}{k} \binom{m}{k} (-4|X|^2)^{n-k} \left(\frac{1}{2}\right)^{n-k} k! = n! L_n^{m-n}(2|X|^2) \quad (\text{A.10})$$

$$S = \sum_{k=0}^n \frac{n!}{(n-k)!} \binom{m}{k} (-2|X|^2)^{n-k} \quad (\text{A.11})$$

By definition the generalised Laguerre polynomial is given by:

$$L_n^{k'}(x) = \frac{1}{n!} \sum_{i=0}^n \frac{n!}{i!} \binom{n+k'}{n-i} (-x)^i \Leftrightarrow \frac{1}{n!} \sum_{i=n}^0 \frac{n!}{(n-i)!} \binom{n+k'}{i} (-x)^{n-i} \quad (\text{A.12})$$

Where on the right hand side of (A.12) the sum is in reversed order.

$$L_n^{k'}(x) = \frac{1}{n!} \sum_{i=0}^n \frac{n!}{(n-i)!} \binom{n+k'}{i} (-x)^{n-i} \quad (\text{A.13})$$

S in (A.11) is equivalent to (A.13). Integer m in (A.11) corresponds to $n+k'$ in (A.13), integer k in (A.11) corresponds to i in (A.13) and n is the same index in both expressions. Hence the equality in (A.10) is shown to be true.

A.2 Wigner Function for two Harmonic Oscillators

Using the results above one can calculate the Wigner Distribution for, *e.g.*, two harmonic oscillators

$$W(x_1, p_1, x_2, p_2) = W(x_1, p_1) W(x_2, p_2).$$

The wave function in the number basis for this system is $|\psi\rangle = \sum_{n_1 n_2} \alpha_{n_1 n_2} |n_1 n_2\rangle$. From (A.2) the expression for the Wigner function becomes

$$W(x_1, p_1, x_2, p_2) = \sum_{n_1, m_1} \sum_{n_2, m_2} \alpha_{n_1 n_2} \alpha_{m_1 m_2}^* \mathcal{W}_{n_1 m_1}(x_1, p_1) \mathcal{W}_{n_2 m_2}(x_2, p_2),$$

where $\mathcal{W}_{n_1 m_1}(x_1, p_1)$ and $\mathcal{W}_{n_2 m_2}(x_2, p_2)$ are the Moyal functions given by (A.4). As mentioned earlier, by performing integration over certain variables, one obtains the Wigner distribution for the remaining ones. Hence the reduced Wigner distributions for oscillator 1 and 2 are obtained by the integrations

$$\begin{aligned} W(x_1, p_1) &= \int_{-\infty}^{\infty} \int_{-\infty}^{\infty} W(x_1, p_1, x_2, p_2) dx_2 dp_2, \\ W(x_2, p_2) &= \int_{-\infty}^{\infty} \int_{-\infty}^{\infty} W(x_1, p_1, x_2, p_2) dx_1 dp_1. \end{aligned} \tag{A.14}$$

APPENDIX B

Rotating Wave Approximation

The purpose of the rotating wave approximation (RWA) is to simplify the system Hamiltonian by removing the rapidly oscillating terms from its interaction picture representation. The interaction picture is a frame where only the interaction part of the Hamiltonian is taken into account. This is often convenient for analysis.

As an example assume a system Hamiltonian of two interacting oscillators $\hat{H} = \hat{H}_0 + \hat{H}_I$. The Hamiltonian is time *independent*, \hat{H}_0 is the diagonal part in a certain basis and \hat{H}_I represents the interaction between the oscillators. The initial state in the Schrödinger picture is $|\psi(t=0)\rangle_S = |\psi_0\rangle$. The time evolution obtained by solving the Schrödinger equation, $i\hbar\partial_t|\psi\rangle = \hat{H}|\psi\rangle$, is given by

$$|\psi(t)\rangle_S = e^{-i\hat{H}t/\hbar}|\psi_0\rangle.$$

By definition the transformation between the Schrödinger and the interaction picture is

$$|\psi\rangle_S = e^{-i\hat{H}_0t/\hbar}|\psi\rangle_I, \quad (\text{B.1})$$

where for $t=0$ the initial states are equal in both representations, $|\psi(t=0)\rangle_S = |\psi(t=0)\rangle_I = |\psi_0\rangle$.

The time evolution in the interaction picture is obtained by solving the Schrödinger equation

$$i\hbar\partial_t \left[e^{-i\hat{H}_0t/\hbar}|\psi\rangle_I \right] = (\hat{H}_0 + \hat{H}_I)e^{-i\hat{H}_0t/\hbar}|\psi\rangle_I,$$

which can be shown is equivalent to

$$i\hbar\partial_t|\psi\rangle_I = e^{i\hat{H}_0t/\hbar}\hat{H}_Ie^{-i\hat{H}_0t/\hbar}|\psi\rangle_I = \hat{H}_I(t)|\psi\rangle_I. \quad (\text{B.2})$$

This is the equation of time evolution in the interaction picture and $\hat{H}_I(t)$ is the time *dependent* interaction picture operator. Due to this dependence the exact solution of (B.2) is given by

$$|\psi(t)\rangle_I = \hat{T}e^{-i/\hbar \int_0^t dt' \hat{H}_I(t')}|\psi_0\rangle. \quad (\text{B.3})$$

Here \hat{T} is the time order product operator, and the formal solution of $\hat{T}e^{-i \int_0^t dt' \hat{H}_I(t')}$ is given in terms of the Dyson series [69].

Instead of solving complicated integrals one can approximate the solution by performing the Rotating Wave Approximation. The rapidly oscillating terms with unequal numbers of creation and annihilation operators are omitted from the interaction picture Hamiltonian, so that it is constant in time, $\hat{H}_I(t) \approx \hat{H}_{\text{I RWA}}$. The solution of (B.3) is then approximated by

$$|\psi(t)\rangle_I \approx e^{-(i\hat{H}_{\text{I RWA}}t)/\hbar}|\psi_0\rangle.$$

To illustrate the approximation, assume the Hamiltonian is

$$\hat{H} = \hbar\omega(\hat{a}_1^\dagger\hat{a}_1 + \hat{a}_2^\dagger\hat{a}_2) + \chi(\hat{a}_1^\dagger + \hat{a}_1)^2(\hat{a}_2^\dagger + \hat{a}_2)^2,$$

where the first bracket represents \hat{H}_0 and the second represents \hat{H}_I . Here ω is the oscillation frequency of both oscillators and χ is the nonlinearity. The ladder operators evolve as $\hat{a}_{1,2}^\dagger(t) = \hat{a}_{1,2}^\dagger e^{i\omega t}$, $\hat{a}_{1,2}(t) = \hat{a}_{1,2} e^{-i\omega t}$, where $e^{\mp i\omega t}$ are rapidly oscillating factors. In even terms of \hat{H}_I the rapid oscillations of $\hat{a}_{1,2}(t)$ and $\hat{a}_{1,2}^\dagger(t)$ cancel each other. Hence the RWA interaction Hamiltonian is

$$\hat{H}_{\text{I RWA}} = \chi(\hat{a}_1^\dagger\hat{a}_1\hat{a}_2\hat{a}_2^\dagger + \hat{a}_1^\dagger\hat{a}_1\hat{a}_2^\dagger\hat{a}_2 + \hat{a}_1\hat{a}_1^\dagger\hat{a}_2\hat{a}_2^\dagger + \hat{a}_1\hat{a}_1^\dagger\hat{a}_2^\dagger\hat{a}_2),$$

and the approximated evolution of the system's state vector is given by $|\psi(t)\rangle_I \approx e^{-i\hat{H}_{\text{I RWA}}t/\hbar}|\psi_0\rangle$.

The difference between the Schrödinger representation and the interaction picture RWA is noticeable when performing a Wigner function analysis. During a time evolution by the complete Hamiltonian, the Wigner function will rapidly rotate in its phase space in addition to changing its shape due to the nonlinear terms. In interaction picture RWA the Wigner function will stand still in phase space, while its shape slowly changes.

APPENDIX C

Evolution of a Coherent State in a Duffing Potential

Here it is shown how an initial coherent state $|\alpha\rangle$ transforms into a Yurke-Stoler cat state, when evolving freely in a Duffing potential.

The time evolution of $|\alpha\rangle$ in a harmonic potential is well known, $|\alpha(t)\rangle = |\alpha e^{-i\omega t}\rangle$ so a study of anharmonic effects suffices to treating the Yurke-Stoler Hamiltonian (2.13) in the interaction picture. From now, all the operators and states are hence in the interaction picture.

The Duffing Hamiltonian

$$\hat{H} = \hbar\mu\hat{n}^2 \quad (\text{C.1})$$

is diagonal in the number basis, so $|\alpha\rangle$ can also be expressed in the number basis. The time evolution under (C.1) is

$$|\alpha(t)\rangle = e^{-i\hat{H}t/\hbar}|\alpha\rangle = e^{-|\alpha|^2/2} \sum_{n=0}^{\infty} \frac{\alpha^n}{\sqrt{n!}} e^{-i\mu n^2 t} |n\rangle. \quad (\text{C.2})$$

In contrast to the case of coherent evolution in a harmonic potential, it is not possible to reformulate the sum in (C.2) in terms of $|\alpha\rangle$ for a general time t . However, there exist special times $t \in [\frac{T}{4}, \frac{T}{2}, \frac{3T}{4}, T]$, where $T = 2\pi/\mu$, for which (C.2) simplifies.

First the simplest cases will be treated. For time $t = T = 2\pi/\mu$ one has that

$$|\alpha(t = 2\pi/\mu)\rangle = e^{-|\alpha|^2/2} \sum_{n=0}^{\infty} \frac{\alpha^n}{\sqrt{n!}} e^{-i2\pi n^2} |n\rangle, \quad (\text{C.3})$$

$$e^{-i2\pi n^2} = \cos(2\pi n^2) - i \sin(2\pi n^2) = 1, \quad n = 0, 1, 2, 3, \dots, \quad (\text{C.4})$$

so that $|\alpha(t = 2\pi/\mu)\rangle = |\alpha(t = 0)\rangle$. After one period the state is the initial coherent state.

For time $t = T/2 = \pi/\mu$ one has that

$$|\alpha(t = 2\pi/\mu)\rangle = e^{-|\alpha|^2/2} \sum_{n=0}^{\infty} \frac{\alpha^n}{\sqrt{n!}} e^{-i\pi n^2} |n\rangle, \quad (\text{C.5})$$

$$e^{-i\pi n^2} = \cos(\pi n^2) - i \sin(\pi n^2) = (-1)^n, \quad n = 0, 1, 2, 3, \dots, \quad (\text{C.6})$$

so that $|\alpha(t = \pi/\mu)\rangle = |-\alpha(t = 0)\rangle$. After half a period the state is the initial coherent state, but with a negative amplitude.

For time $t = T/4 = \pi/2\mu$ one has

$$|\alpha(t = \pi/2\mu)\rangle = e^{-|\alpha|^2/2} \sum_{n=0}^{\infty} \frac{\alpha^n}{\sqrt{n!}} e^{-i\frac{\pi}{2}n^2} |n\rangle, \quad (\text{C.7})$$

$$e^{-i\frac{\pi}{2}n^2} = \cos\left(\frac{\pi n^2}{2}\right) - i \sin\left(\frac{\pi n^2}{2}\right) = \begin{cases} 1 & n = \text{even}, \\ -i & n = \text{odd}. \end{cases}$$

The sum in (C.7) can be split into sums over even (real) and odd (imaginary) entries

$$|\alpha(t = \pi/2\mu)\rangle = e^{-\alpha^2/2} \left[\sum_{n=\text{even}} \frac{\alpha^n}{\sqrt{n!}} |n\rangle + i \sum_{n=\text{odd}} \frac{(-\alpha)^n}{\sqrt{n!}} |n\rangle \right]. \quad (\text{C.8})$$

The sum in (C.8) can be rewritten in terms of coherent states by letting the summation index run over all n , and accordingly including phase factors¹ $e^{\pm i\pi/4}$. The state in (C.8) is equivalent to the Yurke-Stoler cat state

$$|\alpha(t = \pi/2\mu)\rangle = e^{-\alpha^2/2} \left[\sum_{n=0}^{\infty} e^{-i\pi/4} \frac{\alpha^n}{\sqrt{n!}} |n\rangle + e^{i\pi/4} \frac{(-\alpha)^n}{\sqrt{n!}} |n\rangle \right] = \frac{e^{-i\pi/4}}{\sqrt{2}} [|\alpha\rangle + i|-\alpha\rangle]. \quad (\text{C.9})$$

The prefactor $1/\sqrt{2}$ is due to renormalization.

¹Coherent states have both odd and even entries. If the summation index is altered to be over all n , terms with odd real entries and even imaginary entries are added to the sums in (C.8). This changes the state. These additional terms are removed by inclusion of the phase factors.

APPENDIX D

Quantum Master Equations

This appendix considers the derivation of the Born-Markov quantum master equation within the quantum optical limit. First the derivation of the general QME will be given, then in section D.1 the general equation will be applied to a harmonic oscillator system linearly coupled to a bath. Further, a derivation of a harmonic oscillator nonlinearly coupled to a bath will be given in section D.2.

Consider a system weakly coupled to an environment with a large number of harmonic modes. The total Hamiltonian of the system and the bath is

$$H = H_S + H_B + H_{SB}, \quad (\text{D.1})$$

where H_S is the system Hamiltonian, H_B is the Hamiltonian of the bosonic bath and H_{SB} is the interaction between the system and the bath. For simplicity the operators do not have a "hat" in their notation.

The von Neumann equation of motion of the total density matrix ρ in the interaction picture is

$$\dot{\rho}(t) = -i[H_{SB}(t), \rho(t)], \quad (\text{D.2})$$

where

$$H_{SB}(t) = \sum_{\alpha} A_{\alpha}(t) \otimes B_{\alpha}(t) \quad (\text{D.3})$$

is the general interaction with the standard transformation between the interaction and Schrödinger frames

$$A_{\alpha}(t) = e^{iH_S t} A_{\alpha} e^{-iH_S t}, \quad B_{\alpha}(t) = e^{iH_B t} B_{\alpha} e^{-iH_B t}. \quad (\text{D.4})$$

The solution of (D.2) is

$$\rho(t) = \rho(t_0) - i \int_{t_0}^t ds [H_{SB}(s), \rho(s)]. \quad (\text{D.5})$$

By inserting (D.5) into (D.2), one obtains

$$\dot{\rho}(t) = -i[H_{SB}(t), \rho(t_0)] - i[H_{SB}(t), -i \int_{t_0}^t ds [H_{SB}(s), \rho(s)]]. \quad (\text{D.6})$$

The first commutator term in (D.6) can be set to zero by the assumption that at t_0 the system is in thermal equilibrium in the vast past, and the interaction between the system and the bath has not yet begun. By performing the Born approximation the system-bath coupling is assumed to be weak, so that the bath is not affected by any changes in the system. Additionally, the bath is assumed to be in its equilibrium state, so that the total density matrix can be approximated by

$$\rho(s) \approx \rho_S(s) \otimes \rho_B. \quad (\text{D.7})$$

The bath degrees of freedom can be traced over and the QME becomes

$$\dot{\rho}_S(t) = - \int_{t_0}^t ds Tr_B [H_{SB}(t), [H_{SB}(s), \rho_S(s) \otimes \rho_B]]. \quad (\text{D.8})$$

The Markov approximation means that the state of the system does not depend on the past, *i.e.*, the system has no memory of the past

$$\rho_S(s) \rightarrow \rho_S(t). \quad (\text{D.9})$$

By assuming that the past happened a long time ago, the integral limits can be adjusted by the variable change $\tau = t - s$, $d\tau = -ds$, and setting $t_0 = -\infty$. The general interaction picture Markovian quantum master equation then obtains the form

$$\dot{\rho}_S(t) = - \int_0^\infty d\tau Tr_B [H_{SB}(t), [H_{SB}(t - \tau), \rho_S(t) \otimes \rho_B]]. \quad (\text{D.10})$$

Inserting (D.3) into (D.10) the QME is

$$\dot{\rho}_S(t) = - \int_0^\infty d\tau Tr_B \left[\sum_\alpha A_\alpha(t) \otimes B_\alpha(t), \left[\sum_\beta A_\beta(t - \tau) \otimes B_\beta(t - \tau), \rho_S(t) \rho_B \right] \right]. \quad (\text{D.11})$$

After rearranging the terms, extracting the possible factors from the trace and performing cyclic permutation inside the trace brackets, the expression within the outer brackets of (D.11) is

$$\begin{aligned} & \sum_{\alpha, \beta} \left[A_\alpha(t) A_\beta(t - \tau) \rho_S(t) - A_\beta(t - \tau) \rho_S(t) A_\alpha(t) \right] Tr_B \{ B_\alpha(t) B_\beta(t - \tau) \rho_B \} \\ & + \left[\rho_S(t) A_\beta(t - \tau) A_\alpha(t) - A_\alpha(t) \rho_S(t) A_\beta(t - \tau) \right] Tr_B \{ B_\beta(t - \tau) B_\alpha(t) \rho_B \}, \end{aligned}$$

where the traces

$$\begin{aligned} Tr_B \{ B_\alpha(t) B_\beta(t - \tau) \rho_B \} &= \langle B_\alpha(t) B_\beta(t - \tau) \rangle_B = C_{\alpha\beta}(t, t - \tau), \\ Tr_B \{ B_\beta(t - \tau) B_\alpha(t) \rho_B \} &= \langle B_\beta(t - \tau) B_\alpha(t) \rangle_B = C_{\beta\alpha}(t - \tau, t), \end{aligned} \quad (\text{D.12})$$

are the bath correlation functions. Since the assumption of thermal equilibrium was applied, by cyclic permutation the functions in (D.12) can be expressed as

$$\begin{aligned} C_{\alpha\beta}(t, t - \tau) &= \langle B_\alpha(\tau) B_\beta(0) \rangle_B = C_{\alpha\beta}(\tau) \\ C_{\beta\alpha}(t - \tau, t) &= \langle B_\beta(-\tau) B_\alpha(0) \rangle_B = C_{\beta\alpha}(-\tau). \end{aligned} \quad (\text{D.13})$$

Inserting (D.13) into (D.11), the general expression of the Born-Markov QME in the interaction picture is

$$\begin{aligned} \dot{\rho}_S(t) &= - \sum_{\alpha, \beta} \int_0^\infty d\tau \left[A_\alpha(t) A_\beta(t - \tau) \rho_S(t) - A_\beta(t - \tau) \rho_S(t) A_\alpha(t) \right] C_{\alpha\beta}(\tau) \\ &\quad + \left[\rho_S(t) A_\beta(t - \tau) A_\alpha(t) - A_\alpha(t) \rho_S(t) A_\beta(t - \tau) \right] C_{\beta\alpha}(-\tau). \end{aligned} \quad (\text{D.14})$$

D.1 Linear Coupling

The total Hamiltonian of the harmonic oscillator linearly coupled to a bath of harmonic modes is

$$H = \omega_0 a^\dagger a + \sum_k \omega_k b_k^\dagger b_k + (a^\dagger + a) \sum_k g_k b_k^\dagger + g_k^* b_k,$$

where ω_0 is the oscillator frequency and $a(a^\dagger)$ are its annihilation and creation operators. The operators $b_k(b_k^\dagger)$ are annihilation and creation operators of the k 'th bath mode with the corresponding frequency ω_k . The coupling strength of the k 'th bath mode to the oscillator is denoted by g_k , and $\hbar = 1$. The interaction operators are

$$A(t) = a^\dagger e^{i\omega_0 t} + a e^{-i\omega_0 t}, \quad B(t) = \sum_k g_k b_k^\dagger e^{i\omega_k t} + g_k^* b_k e^{-i\omega_k t}. \quad (\text{D.15})$$

Introducing $A(t)$ into (D.14) and discarding the rapidly oscillating terms with factors of $e^{\pm 2i\omega_0 t}$, the QME is

$$\begin{aligned} \dot{\rho}_S(t) &= \int_0^\infty d\tau C(\tau) e^{i\omega_0 \tau} (a^\dagger a \rho_S - a \rho_S a^\dagger) \\ &\quad + \int_0^\infty d\tau C(-\tau) e^{-i\omega_0 \tau} (\rho_S a^\dagger a - a \rho_S a^\dagger) \\ &\quad + \int_0^\infty d\tau C(\tau) e^{-i\omega_0 \tau} (a a^\dagger \rho_S - a \rho_S a^\dagger) \\ &\quad + \int_0^\infty d\tau C(-\tau) e^{i\omega_0 \tau} (\rho_S a a^\dagger - a^\dagger \rho_S a). \end{aligned} \quad (\text{D.16})$$

By defining the one-sided Fourier transforms

$$\begin{aligned}\Gamma_+(\omega) &= \int_0^\infty d\tau C(\tau)e^{i\omega\tau}, \\ \Gamma_-(\omega) &= \int_0^\infty d\tau C(-\tau)e^{i\omega\tau} = \int_{-\infty}^0 d\tau C(\tau)e^{-i\omega\tau}, \\ \Gamma_+(-\omega) &= \int_0^\infty d\tau C(\tau)e^{-i\omega\tau} = \int_{-\infty}^0 d\tau C(-\tau)e^{i\omega\tau}, \\ \Gamma_-(-\omega) &= \int_0^\infty d\tau C(-\tau)e^{-i\omega\tau} = \int_{-\infty}^0 d\tau C(\tau)e^{i\omega\tau},\end{aligned}\tag{D.17}$$

and their linear combinations

$$\begin{aligned}\gamma(\omega) &= \Gamma_+(\omega) + \Gamma_-(-\omega) = \int_{-\infty}^\infty d\tau C(\tau)e^{i\omega\tau}, \\ \gamma(-\omega) &= \Gamma_+(-\omega) + \Gamma_-(\omega) = \int_{-\infty}^\infty d\tau C(\tau)e^{-i\omega\tau}, \\ 2iS(\omega) &= \Gamma_+(\omega) - \Gamma_-(-\omega), \\ 2iS(-\omega) &= \Gamma_+(-\omega) - \Gamma_-(\omega).\end{aligned}\tag{D.18}$$

equation (D.16), when $\omega = \omega_0$, is

$$\begin{aligned}\dot{\rho}_S &= -i[S(\omega_0)[a^\dagger a, \rho_S(t)] + S(-\omega_0)[aa^\dagger, \rho_S(t)]] + \\ &\gamma(\omega_0)[a\rho_S a^\dagger - \frac{1}{2}\{a^\dagger a, \rho_S(t)\}] + \gamma(-\omega_0)[a^\dagger \rho_S a - \frac{1}{2}\{aa^\dagger, \rho_S(t)\}].\end{aligned}\tag{D.19}$$

The first bracket is the Lamb shift, which is a shift of the oscillator's frequency due to the system-bath interaction. The rest of the terms constitute the Lindblad superoperator in (3.9).

The dissipation rate can now be calculated. By the definition in (D.12) and (D.13) the bath correlation functions are

$$C(\pm\tau) = \sum_k |g_k|^2 [\langle b_k^\dagger b_k \rangle e^{\pm i\omega_k \tau} + \langle b_k b_k^\dagger \rangle e^{\mp i\omega_k \tau}],\tag{D.20}$$

where it has been assumed that the modes are non-interacting and the self-correlation $\langle b_k^\dagger b_k^\dagger \rangle = \langle b_k b_k \rangle = 0$. The dissipation rate is then

$$\begin{aligned}\gamma(\omega_0) &= \sum_k |g_k|^2 \left[\langle b_k^\dagger b_k \rangle \int_{-\infty}^\infty d\tau e^{i(\omega_k + \omega_0)\tau} + \langle b_k b_k^\dagger \rangle \int_{-\infty}^\infty d\tau e^{i(-\omega_k + \omega_0)\tau} \right] \\ &= \sum_k |g_k|^2 [N_B(\omega_k)\delta(\omega_k + \omega_0) + [N_B(\omega_k) + 1]\delta(\omega_0 - \omega_k)]\end{aligned}\tag{D.21}$$

$$= \sum_k |g_k|^2 \delta(\omega_0 - \omega_k) [N_B(\omega_k) + 1]\tag{D.22}$$

$$= \Gamma_0 [N_B(\omega_0) + 1],\tag{D.23}$$

where $N_B(\omega_k)$ is the Bose Einstein distribution, the spectral density of the bath is assumed to be Ohmic $\sum_k |g_k|^2 \delta(\omega - \omega_k) = \Gamma_0 \omega / \omega_0$, and Γ_0 is the linear dissipation strength. It is also assumed that $\omega_k \geq 0$. By similar approach, the excitation rate is $\gamma(-\omega_0) = \Gamma_0 N_B(\omega_0)$.

D.2 Nonlinear coupling

In the same manner as above one can derive the QME for a harmonic oscillator nonlinearly coupled to the bosonic bath. The total Hamiltonian is as in (D.15), only with a quadratic coupling between the oscillator and the bath

$$H_{\text{SB}} = (a^\dagger + a)^2 \sum_k \eta_k b_k^\dagger + \eta_k^* b_k. \quad (\text{D.24})$$

The interaction picture operators are $A(t) = (a^\dagger e^{i\omega_0 t} + a e^{-i\omega_0 t})^2$ and $B(t)$ is as in (D.15), with the coupling strength η_k of the oscillator to the k 'th bath mode. By the same procedure as in the previous section, introducing $A(t)$ into the general QME (D.10), discarding the terms with rapidly oscillating factors of $e^{\pm 4i\omega_0 t}$, and applying the definitions in (D.17) and (D.18), the QME is

$$\dot{\rho}_{\text{S}} = -2i \left[S(2\omega_0) [a^{\dagger 2} a^2, \rho_{\text{S}} + S(-2\omega_0) [a^2 a^{\dagger 2}, \rho_{\text{S}}]] + \right. \quad (\text{D.25})$$

$$\left. \gamma(2\omega_0) \left[a^2 \rho_{\text{S}} a^{\dagger 2} - \frac{1}{2} \{ a^{\dagger 2} a^2, \rho_{\text{S}} \} + \right. \right. \quad (\text{D.26})$$

$$\left. \gamma(-2\omega_0) \left[a^{\dagger 2} \rho_{\text{S}} a^2 - \frac{1}{2} \{ a^2 a^{\dagger 2}, \rho_{\text{S}} \} \right] - \right. \quad (\text{D.27})$$

$$\left. \left[2iS(0) [(2a^\dagger a + 1)^2, \rho_{\text{S}}] + \gamma(0) \{ (2a^\dagger a + 1)^2, \rho_{\text{S}} \} - \right. \right. \quad (\text{D.28})$$

$$\left. \left. \gamma(0) (4a^\dagger a \rho_{\text{S}} a^\dagger a + \{ a^\dagger a, \rho_{\text{S}} \} + \rho_{\text{S}}) \right].$$

The first bracket in (D.25) is the Lamb shift, introducing a renormalization of the oscillator's Duffing constant due to the system-bath interaction. The second and third brackets are the terms of the Lindblad superoperator in (3.14). The remaining terms are non-physical and can be omitted.

The calculation of the dissipation rate follows the same procedure as in section D.1. The correlation functions are

$$C(\pm\tau) = \sum_k |\eta_k|^2 \left[\langle b_k^\dagger b_k \rangle e^{\pm i\omega_k \tau} + \langle b_k b_k^\dagger \rangle e^{\mp i\omega_k \tau} \right], \quad (\text{D.29})$$

where it has been assumed that the modes are non-interacting and the self-correlation $\langle b_k^\dagger b_k^\dagger \rangle = \langle b_k b_k \rangle = 0$. The dissipation rate is then

$$\begin{aligned} \gamma(2\omega_0) &= \sum_k |\eta_k|^2 \left[\langle b_k^\dagger b_k \rangle \int_{-\infty}^{\infty} d\tau e^{i(\omega_k + 2\omega_0)\tau} + \langle b_k b_k^\dagger \rangle \int_{-\infty}^{\infty} d\tau e^{i(-\omega_k + 2\omega_0)\tau} \right] \\ &= \sum_k |\eta_k|^2 \left[N_{\text{B}}(\omega_k) \delta(\omega_k + 2\omega_0) + [N_{\text{B}}(\omega_k) + 1] \delta(2\omega_0 - \omega_k) \right] \quad (\text{D.30}) \end{aligned}$$

$$= \sum_k |\eta_k|^2 \delta(2\omega_0 - \omega_k) [N_{\text{B}}(\omega_k) + 1] \quad (\text{D.31})$$

$$= \Gamma [N_{\text{B}}(2\omega_0) + 1], \quad (\text{D.32})$$

where $N_{\text{B}}(\omega_k)$ is the Bose Einstein distribution, the spectral density of the bath is assumed to be Ohmic $\sum_k |\eta_k|^2 \delta(\omega - \omega_k) = \Gamma\omega/2\omega_0$, and Γ is the nonlinear dissipation strength. It is also assumed that $\omega_k \geq 0$. The excitation rate $\gamma(-2\omega_0) = \Gamma N_{\text{B}}(2\omega_0)$ can be obtained by the same approach.

BIBLIOGRAPHY

- [1] M. Planck. Ueber Irreversible Strahlungsvorgänge. *Ann. Phys*, **306** , 1900.
- [2] H. Herz. Ueber einen Einfluss des ultravioletten Lichtes auf die electrische Entladung. *Ann. Phys*, **267** , 1887.
- [3] A. Einstein. Concerning a Heuristic Point of View Toward the Emission and Transformation of Light. *Ann. Phys*, **17** , 1905.
- [4] W. P. Schleich. *Quantum Optics in Phase Space*. Wiley-VCH, Berlin, 2001.
- [5] V. V. Dodonov. Nonclassical States in Quantum Optics: A Squeezed Review of the First 75 Years. *J. Opt. B*, **4** , 2002.
- [6] S. Haroche. Nobel Lecture: Controlling Photons in a Box and Exploring the Quantum to Classical Boundary. The Nobel Foundation, 2012.
- [7] T. W. Hänsch and H. Walther. Laser Spectroscopy and Quantum Optics. *Rev. Mod. Phys*, **71** , 1999.
- [8] V. B. Braginsky and F.Y. Khalili. Quantum Nondemolition Measurements: the Route From Toys to Tools. *Rev. Mod. Phys.*, **68** (1), 1996.
- [9] P. Nussenzveig et al. Preparation of High-Principal-Quantum-Number Circular States of Rubidium. *Phys. Rev. A*, **48** (5), 1993.
- [10] D. Meschede et al. One-Atom Maser. *Phys. Rev. Lett.*, **54** (6), 1985.
- [11] D. J. Wineland. Nobel Lecture: Superposition, entanglement, and Raising Schrödinger's Cat. *Rev. Mod. Phys.*, **85** (3), 2013.
- [12] C. Monroe et al. A Schrödinger Cat Superposition State of an Atom. *Science*, **272** , 1996.
- [13] S. Haroche et al. Atomic Clocks for Controlling Light Fields. *Phys. Today*, **66** (1), 2013.
- [14] D. T. Smithey et al. Measurement of the Wigner distribution and the density matrix of a light mode using optical homodyne tomography: Application to squeezed states and the vacuum. *Phys. Rev. Lett.*, **70** (9), 1993.

- [15] G. Adesso and F. Illuminati. Entanglement in Continuous Variable Systems: Recent Advances and Current Perspectives. *J. Phys. A: Math. Theor.*, **40** , 2007.
- [16] J. I. Latorre and A. Riera. A Short Review on Entanglement in Quantum Spin Systems. *J. Phys. A: Math. Theor.*, **42** , 2009.
- [17] T. A. Palomaki et al. Entangling Mechanical Motion with Microwave Fields. *Science*, **342** , 2013.
- [18] J. R. Friedman et al. Quantum Superposition of Distinct Macroscopic States. *Nature*, **406** , 2000.
- [19] M. Arndt et al. Wave-particle duality of C_{60} molecules. *Nature*, **401** , 1999.
- [20] S. Gerlich et al. Quantum Interference of Large Organic Molecules. *Nature Communications*, **2** , 2011.
- [21] O. Romero-Isart et al. Toward Quantum Superposition of Living Organisms. *New Journal of Physics*, **12** , 2010.
- [22] A. D. O'Connell et al. Quantum Ground State and Single-Phonon Control of a Mechanical Resonator. *Nature*, **464** , 2010.
- [23] J. D. Teufel et al. Circuit cavity electromechanics in the strong-coupling regime. *Nature*, **471** , 2011.
- [24] M. Poot and H. S. J. van der Zant. Mechanical Systems in the Quantum Regime. *Physics Reports*, **511** (5), 2012.
- [25] M. Aspelmeyer et al. Cavity Optomechanics. arXiv:1303.0733, 2013.
- [26] J. D. Teufel et al. Sideband Cooling of Micromechanical Motion to the Quantum Ground State. *Nature*, **475** , 2011.
- [27] A. K. Hüttel et al. Carbon Nanotubes as Ultrahigh Quality Factor Mechanical Resonators. *Nano Letters*, **9** , 2009.
- [28] A. Eichler et al. Nonlinear Damping in Mechanical Resonators Made from Carbon Nanotubes and Graphene. *Nature Nanotechnology*, **6** , 2011.
- [29] K. S. Novoselov et al. Electric Field Effect in Atomically Thin Carbon Films. *Science*, **306** , 2004.
- [30] K. S. Novoselov A. K. Geim. The Rise of Graphene. *Nature*, **6** , 2007.
- [31] J. Bringham et al. Electric Field Effect in Atomically Thin Carbon Films. *Nature*, **506** , 214.

- [32] J. Atalaya et al. Continuum Elastic Modeling of Graphene Resonators. *Nano Letters*, **8** , 2008.
- [33] A. M. v d et al. Large-Scale Arrays of Single-Layer Graphene Resonators. *Nanoletters*, **10** , 2010.
- [34] C. Chen et al. Graphene Mechanical Oscillators with Tunable Frequency. *Nature Nanotechnology*, **8** , 2013.
- [35] I. Katz et al. Classical to Quantum Transition of a Driven Nonlinear Nanomechanical Resonator. *New Journal of Physics*, **10** , 2008.
- [36] P. Weber et al. Coupling Graphene Mechanical Resonators to Superconducting Microwave Cavities. *Nanoletters*, **14** , 2014.
- [37] X. Song et al. Graphene Optomechanics Realized at Microwave Frequencies. *Phys. Rev. Lett.*, **113** (2), 2014.
- [38] V. Singh et al. Optomechanical Coupling Between a Multilayer Graphene Mechanical Resonator and a superconducting Microwave Cavity. *Nature Nanotechnology*, **9** , 2014.
- [39] A. Croy et al. Nonlinear Damping in Graphene Resonators. *Phys. Rev. B*, **86** , 2012.
- [40] M. Imboden and P. Mohanty. Dissipation in Nanoelectromechanical Systems. *Physics Reports*, **534** (3), 2014.
- [41] L. Gilles and P. Knight. Two-Photon Absorption and Nonclassical States of Light. *Phys. Rev. A*, **48** , 1993.
- [42] L. Gilles et al. Generation of Nonclassical Light by Dissipative Two-Photon Processes. *Phys. Rev. A*, **49** (4), 1994.
- [43] H. Tan et al. Generation of Macroscopic Quantum Superpositions of Optomechanical Oscillators by Dissipation. *Phys. Rev. A*, **88** (2), 2013.
- [44] M. J. Everitt et al. Engineering Dissipative Channels for Realizing Schrödinger Cats in SQUIDS. *Frontiers in ICT, Quantum Computing*, **1** (1), 2014.
- [45] E .P. Wigner. On the quantum correction for thermodynamic equilibrium. *Phys. Rev.*, **40** , 1932.
- [46] B. Yurke and D. Stoler. Generating Quantum Mechanical Superpositions of Macroscopically Distinguishable States via Amplitude Dispersion. *Physical Review Letters*, **57** , 1986.
- [47] R. Horodecki et al. Quantum Entanglement. *Rev. Mod. Phys.*, **81** , 2009.

- [48] A. Einstein et al. Can Quantum Mechanical Description of Physical Reality Be Considered Complete? *Phys. Rev.*, **47** , 1935.
- [49] E. Schrödinger. Die gegenwärtige Situation der Quantenmechanik. *Naturwissenschaften*, **23** , 1935.
- [50] J. S. Bell. On the Einstein Podolsky Rosen Paradox. *Physics*, **1** , 1964.
- [51] J. F. Clauser S. J. Freedman. Experimental Test of Local Hidden-Variable Theories. *Phys. Rev. Lett.*, **28** , 1972.
- [52] A. Aspect et al. Experimental Tests of Realistic Local Theories via Bell's Theorem. **47** , 1981.
- [53] A. Kronwald et al. Arbitrarily Large Steady-State Bosonic Squeezing via Dissipation. *Phys. Rev. A*, **88** , 2013.
- [54] A. Peres. Separability Criterion for Density Matrices. *Phys. Rev. Lett.*, **77** , 1996.
- [55] L. Duan et al. Inseparability Criterion for Continuous Variable Systems. *Phys. Rev. Lett.*, **84** , 2000.
- [56] R. Simon. Peres-Horodecki Separability Criterion for Continuous Variable Systems. *Phys. Rev. Lett.*, **84** , 2000.
- [57] M. Plenio and S. Virmani. An Introduction to Entanglement Measures. *Quantum Information and Computation Archive*, **7** , 2007.
- [58] G. Vidal and R. F. Werner. Computable Measure of Entanglement. *Phys. Rev. A*, **65** , 2002.
- [59] A. Einstein. Investigations on the Theory of the Brownian Movement. *Annalen der Physik*, **322** (8), 1905.
- [60] H. P. Breuer and F. Petruccione. *The Theory of Open Quantum Systems*. Oxford University Press, 2003.
- [61] U. Weiss. *Quantum Dissipative Systems*. World Scientific, Singapore, 1999.
- [62] G. Lindblad. On the Generators of Quantum Dynamical Semigroups. *Commun. Math. Phys*, **48** (2), 1976.
- [63] D. F. Walls and G. J. Milburn. Effect of Dissipation on Quantum Coherence. *Phys. Rev. A*, **31** (4), 1985.
- [64] C. M. Savage and D. F. Walls. Damping of Quantum Coherence: The Master-Equation Approach. *Phys. Rev. A*, **32** (4), 1985.

- [65] V. Bužek et al. Superpositions of Coherent States: Squeezing and Dissipation. *Phys. Rev. A*, **45** (9), 1992.
- [66] G. J. Milburn and C. A. Holmes. Dissipative Quantum and Classical Liouville Mechanics of the Anharmonic Oscillator. *Phys. Rev. Lett.*, **56** (21), 1986.
- [67] M. Dykman and M. Krivoglaz. Theory of Nonlinear Oscillator Interacting with a Medium. *Soc.Sci.Rev A*, **5** , 1984.
- [68] H. D. Simaan and R. Loudon. Off-Diagonal Density Matrix for Single-Beam Two-Photon Absorbed light. *J. Phys. A: Math. Gen.*, (2), 1978.
- [69] J. J. Sakurai. *Modern Quantum Mechanics*. Addison-Wesley, 1994.

